Insightful Improvement in the Design of Potent Uropathogenic E. coli FimH Antagonists

Leila Mousavifar, Meysam Sarshar, Clarisse Bridot, Daniela Scribano, Cecilia Ambrosi, Anna Teresa Palamara, Gérard Vergoten, Benoît Roubinet, Ludovic Landemarre, Julie Bouckaert, et al.

pharmaceutics

MDPI

Article

Insightful Improvement in the Design of Potent Uropathogenic *E. coli* FimH Antagonists

Leila Mousavifar [1], Meysam Sarshar [2], Clarisse Bridot [3], Daniela Scribano [4], Cecilia Ambrosi [5,6], Anna Teresa Palamara [4,7], Gérard Vergoten [8], Benoît Roubinet [9], Ludovic Landemarre [9], Julie Bouckaert [3,*] and René Roy [1,*]

1 Glycosciences and Nanomaterial Laboratory, Université du Québec à Montréal, Succ. Centre-Ville, P.O. Box 8888, Montréal, QC H3C 3P8, Canada
2 Research Laboratories, Bambino Gesù Children's Hospital, Istituto di Ricovero e Cura a Carattere Scientifico, 00146 Rome, Italy
3 Unité de Glycobiologie Structurale et Fonctionnelle (UGSF), UMR8576 du CNRS, Univ. Lille, 59000 Lille, France
4 Department of Public Health and Infectious Diseases, Sapienza University of Rome, 00185 Rome, Italy
5 Department of Human Sciences and Promotion of the Quality of Life, San Raffaele Roma Open University, 00166 Rome, Italy
6 Istituto di Ricovero e Cura a Carattere Scientifico, San Raffaele Roma, 00166 Rome, Italy
7 Department of Infectious Diseases, National Institute of Health, 00161 Rome, Italy
8 Institut de Chimie Pharmaceutique Albert Lespagnol (ICPAL), Faculté de Pharmacie, University of Lille, 3 Rue du Professeur Laguesse, BP-83, 59006 Lille, France
9 GLYcoDiag, 2 Rue du Cristal, 45100 Orléans, France
* Correspondence: julie.bouckaert@univ-lille.fr (J.B.); roy.rene@uqam.ca (R.R.)

Abstract: Selective antiadhesion antagonists of Uropathogenic *Escherichia coli* (UPEC) type-1 Fimbrial adhesin (FimH) are attractive alternatives for antibiotic therapies and prophylaxes against acute or recurrent urinary tract infections (UTIs) caused by UPECs. A rational small library of FimH antagonists based on previously described *C*-linked allyl α-D-mannopyranoside was synthesized using Heck cross-coupling reaction using a series of iodoaryl derivatives. This work reports two new members of FimH antagonist amongst the above family with sub nanomolar affinity. The resulting hydrophobic aglycones, including constrained alkene and aryl groups, were designed to provide additional favorable binding interactions with the so-called FimH "tyrosine gate". The newly synthesized *C*-linked glycomimetic antagonists, having a hydrolytically stable anomeric linkage, exhibited improved binding when compared to previously published analogs, as demonstrated by affinity measurement through interactions by FimH lectin. The crystal structure of FimH co-crystallized with one of the nanomolar antagonists revealed the binding mode of this inhibitor into the active site of the tyrosine gate. In addition, selected mannopyranoside constructs neither affected bacterial growth or cell viability nor interfered with antibiotic activity. *C*-linked mannoside antagonists were effective in decreasing bacterial adhesion to human bladder epithelial cells (HTB-9). Therefore, these molecules constituted additional therapeutic candidates' worth further development in the search for potent anti-adhesive drugs against infections caused by UPEC.

Keywords: uropathogenic *Escherichia coli* (UPEC); FimH; antagonists; mannosides; glycocomimetics; crystallography; adhesion inhibition; bladder cells; molecular dynamic simulations

check for updates

Citation: Mousavifar, L.; Sarshar, M.; Bridot, C.; Scribano, D.; Ambrosi, C.; Palamara, A.T.; Vergoten, G.; Roubinet, B.; Landemarre, L.; Bouckaert, J.; et al. Insightful Improvement in the Design of Potent Uropathogenic *E. coli* FimH Antagonists. *Pharmaceutics* **2023**, *15*, 527. https://doi.org/10.3390/pharmaceutics15020527

Academic Editor: Ivana Cacciatore

Received: 10 January 2023
Revised: 25 January 2023
Accepted: 2 February 2023
Published: 4 February 2023

1. Introduction

One of the major pathogens responsible for urinary tract infections (UTIs) is uropathogenic *Escherichia coli* (*E. coli*) (UPEC), leading to a major burden in public health [1]. As part of the normal microbiota, *E. coli* exhibits diverse species with a wide spectrum of phenotypes that reside in the large intestine of humans and many animals [2]. Several virulence factors are responsible for the establishment of current infections [2,3]. While *E. coli* mainly live

harmlessly in the gut as their primary niche by establishment of a symbiotic relationship, some strains act as pathogens and cause a variety of enteric and extra-enteric diseases [4–6]. Among these, the adhesion of UPECs to the host uroepithelial tissues is due to the *E. coli* type 1 pili, called FimH, which mediate their attachment in a mannose-dependent interaction [4,5]. FimH adhesin of type 1 fimbriae promotes intestinal colonization by binding to colonic crypts of epithelial cells, facilitating *E. coli* adhesion and invasion to the urinary epithelium, a key player in UPEC pathogenicity [6]. Preventing bacterial FimH adhesion to highly mannosylated glycoprotein uroplakin Ia from bladder cells represents an appealing strategy to control UTIs [4]. Since bacterial adhesion to host cells is a critical and initial step in most infectious diseases, anti-adhesion therapy can effectively compete against antibiotic therapy and is seriously considered for the treatment of acute uncomplicated lower UTIs (AUC) [7–9].

Importantly, the mannose-specific adhesin FimH has an essential hydrophobic binding pocket of non-polar amino acids that surrounds the aglycon portion of α-D-mannopyranoside glycomimetics. These findings have been fully exploited in the design of potent FimH anti-adhesins [10–13]. Glycomimetics are simplified representatives of more complex glycoconjugate structures found in nature. They have been designed to improve carbohydrate-protein binding interactions and to provide better pharmacokinetic and pharmacodynamic properties [14,15].

As alternative therapeutic strategies against UTIs, monomeric mannoside antagonists [15–18] and clusters [19–25] with varied hetero-anomeric linkages *O*-[26–29], *S*-[30–32], or *N*-[33,34] have been developed as appealing candidates. Using a plethora of available crystallographic data, detailed structure-activity relationships (SARs) have been established to provide further insight into the binding mode of *E. coli* FimH. This approach has greatly helped in improving the conception of potent antagonists [4,35–39]. Amid the various α-D-mannopyranoside inhibitors described thus far, *C*-linked glycomimetics residues harboring hydrophobic aglycons are still considered worthy candidates as potent FimH inhibitors. Several of these synthetic candidates showed improved binding affinities and increased hydrolytic stability [30,40,41].

This work describes the synthesis, relative binding affinities, crystallographic data, and anti-adhesive properties of a small library of *C*-linked mannopyranoside inhibitors. The data provide further pivotal insights into the potential of these glycomimetics against UPEC strains and give rise to a solid basis toward the development of new and effective FimH antagonists.

2. Results and Discussion

2.1. Synthesis and Structural Characterization

In previous studies, several aryl *C*-mannopyranosides carrying alkenyl aglycons were shown as promising candidates with excellent binding affinities against *E. coli* FimH [40,41]. However, their poor water solubility has restricted their further development as drug candidates. To address this issue, we propose herein the use of heteroaryl-substituted mannopyranosides based upon numerous available crystallographic data.

The first step toward this next generation of antagonists was the improved preparation of *C*-allyl α-D-mannopyranoside **1** as a key starting material. Compound **1** was obtained by per-*O*-benzoylation of commercially available methyl α-D-mannopyranoside (MeMan) followed by a Hosomi–Sakurai reaction to afford the pure α-anomer **1** [40]. Key precursor **1** was next treated under palladium-catalyzed Heck conditions in the presence of aryl iodides (DMF, TBAB, $NaHCO_3$, $Pd(OAc)_2$, 90 °C, o.n.) to afford a family of (*E*)-linked aryl derivatives (**2**–**10**) in good yields (Scheme 1).

As depicted in Figures S1, S2 and S20, ^{1}H-NMR spectra (600 MHz) of both compounds **2** and **11,** together with detailed 2D NMR spectrum of compound **2,** unambiguously confirmed that all the major compounds were the *trans* stereoisomers. Reliable evidence of this claim was the signal of H-3′ of the alkene that appeared as a doublet at δ 6.67 ppm with a $J_{2',3'}$ = 15.8 Hz and 16 Hz for both compounds **2** and **11**, respectively. Moreover,

the coupling constants for the H4 signal at δ 6.00 ppm (dd, 1H, $J_{3,4}$ = $J_{4,5}$ = 8.5 Hz, H-4) unambiguously indicated a *trans*-diaxial relationship between H3-H4 and H4-H5, thus confirming this series of compounds to be in the proper $^4C_1$ chair conformation.

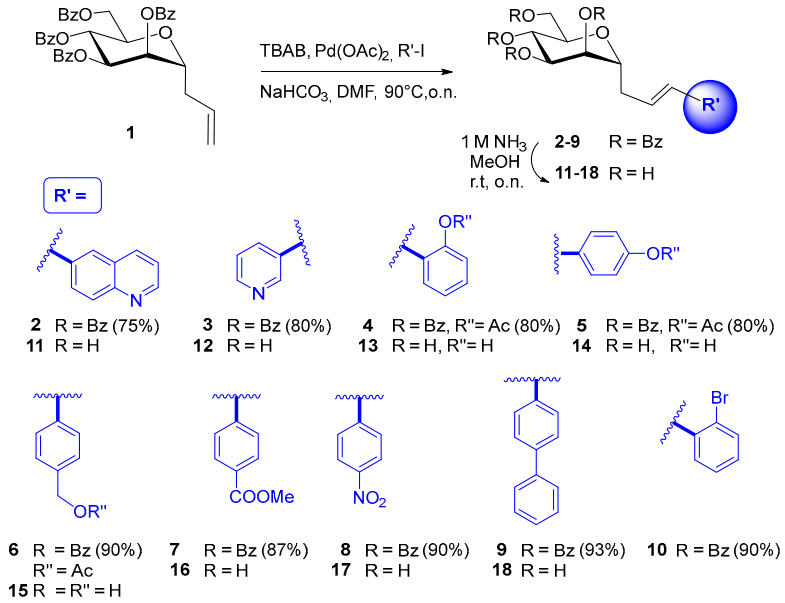

Scheme 1. Synthesis of a family of *C*-linked mannopyranosides using palladium-catalyzed Heck reaction.

Because *C*-linked mannopyranosides do not exhibit an anomeric effect in comparison to their *O*-linked analogs, there was a risk that the analogs had undergone conformational changes from the desired $^4C_1$ chair to skew boats ($^0S_2$ or $_0S^2$) [4]. The X-ray crystal structure of perbenzoylated compound **2** showed it to be in the desired chair conformation as previously observed with several related analogs (Figure S4). Since the conformation of **2** in the solid-state could be different than that in solution, an in-depth NOESY analysis was also performed to further confirm its conformation (Figure S3). The nOe between the geminal H1'a, H1'a' with the axial H3 and H5 unmistakably implied the $^4C_1$ conformation. Analysis of the ^{1}H-NMR spectrum of *C*-linked mannosides (**11**–**18**, and **20**) also showed values of ca. 1.63 Hz for their $^3J_{1,2}$ coupling constants of their vicinal equatorial/axial arrangements (Figure S2).

Finally, benzoyl ester deprotection of *C*-linked mannopyranosides (**2**–**9**) was performed using ammonia in methanol (1M, r.t., o.n.) to provide unprotected derivatives (**11**–**18** and **20**), essentially quantitatively.

2.2. Synthesis of a Key Ortho-Substituted Biphenyl Derivative

In our previous work, an *ortho*-substituted *C*-linked biphenyl mannopyranoside candidate was considered as a promising lead with a K_D of 6.9 nM [41]. Unfortunately, this compound had poor water solubility. To further exploit this promising series of analogs, we envisaged the insertion of heteroaryl moieties at the *ortho* position in order to improve their water-solubility. Hence, compound **10** was synthesized under the above Heck reaction conditions using 1-bromo-2-iodobenzene (DMF, TBAB, $NaHCO_3$, $Pd(OAc)_2$, 90 °C, o.n.). This intermediate was then treated under Suzuki–Miyaura [42,43] coupling conditions using 4-pyridylboronic acid (cesium carbonate, [1,1'-bis(diphenylphosphino)ferrocene] dichloropalladium(II), 80 °C, dioxane/water, 5:1, o.n.) to give compound **19** in 55% yield. Compound **19** was deprotected using a solution of ammonia (1M) in methanol (r.t., o.n.) to afford compound **20** in 80% yield (Scheme 2).

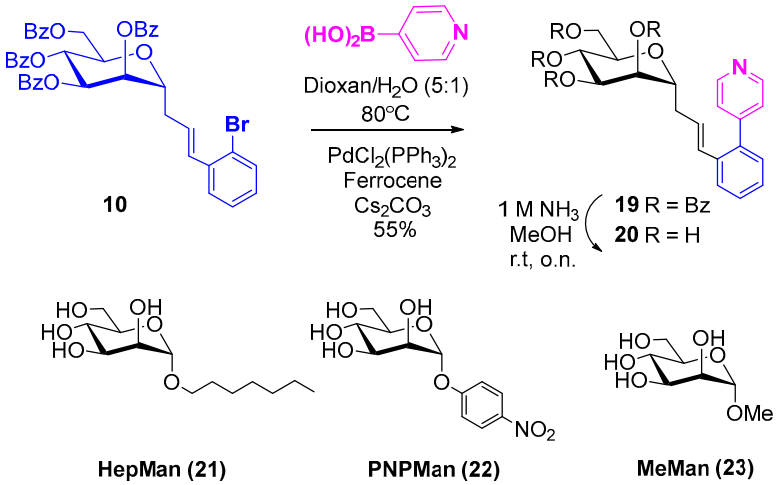

Scheme 2. Synthesis of compound **20** by Suzuki–Miyaura coupling after initial palladium-catalyzed Heck reaction from **10**. Reference standards used in affinity measurements are identified as: HepMan: heptyl α-D-mannopyranoside (**21**); PNPMan (*para*-nitrophenyl α-D-mannopyranoside (**22**); MeMan (methyl α-D-mannopyranoside (**23**).

2.3. Affinity Evaluation of Mannosides through FimH LEctPROFILE Kit

To measure the relative binding affinity of the newly synthesized compounds **11**, **20**, and **18** against FimH, the usual referenced standards were used for comparison with previously published data: heptyl α-D-mannopyranoside (HepMan, **21**), *para*-nitrophenyl α-D-mannopyranoside (PNPMan, **22**), and methyl α-D-mannopyranoside (MeMan, **23**) [4]. The relative inhibitory potential of the above compounds was determined against a biotinylated Man-BSA conjugate using a FimH lectin domain (amino acids 1-158) LEctPROFILE kit (provided by GLYcoDiag) (Figure 1, Table 1). In this assay, IC_{50s} of 19.4 nM, 74.1 nM, and 2810.7 nM, were respectively obtained for **21**, **22**, and **23**. As Figure 1 shows, the best inhibition was obtained from the inhibitor **20**, followed by **11**, and finally the C-linked mannopyranoside **18** with IC_{50s} of 0.82 nM, 3.17 nM, and 30.28 nM, respectively. Undoubtably, the *ortho*-substituted pyridyl derivative **20** is the most efficient monomeric antagonist identified thus far. Interestingly, and as anticipated, compound **20** showed a calculated LogP (cLogP) improved (1.66) in comparison to its fully aromatic counterparts **18** (3.16).

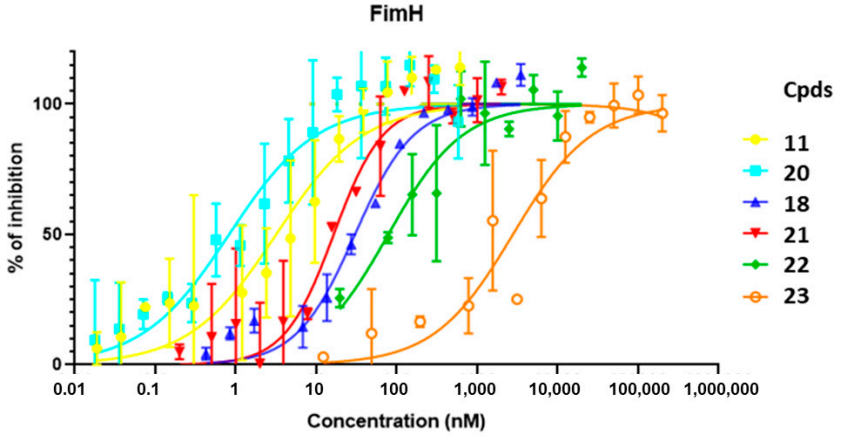

Figure 1. Determination of relative affinity of the lectin binding domain of *E. coli* FimH with mannoside derivatives using solid phase competitive inhibition assay (LEctProfile from GLYcoDiag).

Table 1. Relative binding affinities as measured by FimH LEctPROFILE kit for mannoside derivatives.

Cpd	Structure	IC_{50} (nM)	RIP [a]	cLogP
11	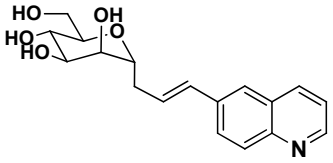	3.17 ± 2.3	887	1.16
18	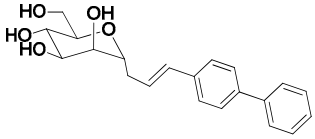	30.28 ± 9.0	93	3.16
20	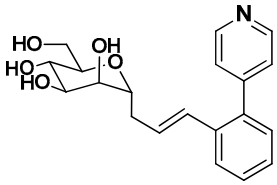	0.82 ± 0.4	3428	1.66
21	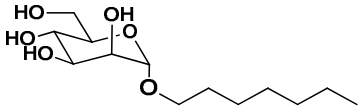	19.4 ± 5.2	145	1.44
22	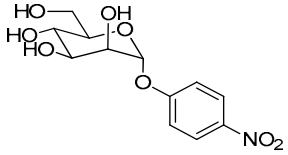	74.13 ± 48.1	38	0.02
23	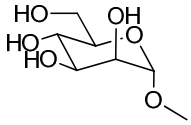	2810.74 ± 2546	1	−1.58

[a] The relative inhibitory potency (RIP) factor obtained by dividing the IC_{50} value of the compounds by the IC_{50} of the reference (MeMan, **23**).

2.4. X-ray and Molecular Dynamic Simulations

Unfortunately, no crystalline structure could be obtained from our best inhibitor **20**. However, co-crystallized FimH with the second-best inhibitor **11** was obtained at a resolution of 3 Å (Figure S38, Table S1, PDB entry code 8BVD). The structure was solved using the PHENIX [44] software to visualize the detailed binding interactions which took place between the FimH binding domain and the inhibitor.

Delightfully, the co-crystal structure of compound **11** and *E. coli* C43 (DE3) FimH [45,46] also revealed the expected $^4C_1$ chair conformation of the ligand **11** bound into the active site of the tyrosine gate. In the mannose-binding site of FimH, we observed Tyr48 in parallel, while the Tyr137 residue was in T-aromatic stacking with the quinoline group of ligand **11**. Four FimH lectin domains were observed in the asymmetric unit of the crystal (Figure S38) and the mannose-binding site of each FimH lectin domain was in proximity with a symmetry-related neighbor in the crystal packing (Figure 2) [34]. The two binding sites of FimH molecules were held together by the two quinoline substituents crossed over in a parallel stacking (Figure 2), while their mannosides projected into the binding pocket of FimH. The distance between the axial O2 hydroxyl group of the non-reducing end mannoside was 12 A° which exactly matched the distance previously observed in

divalently bound trimannoside to FimH (crystal structures with PDB entry codes 6GTV and 6GTW). Therefore, the binding of FimH to compound **11** appeared to simulate the bivalent binding of the natural oligomannosidic *N*-glycan structures [47]. Inhibitor **11** interacted via different amino acids that included Ile 13, Phe 1, Asp 47, Gln 133, Asp 54, Asn 135, Asp 140, Phe 142 in the open conformation of FimH (Figure 3).

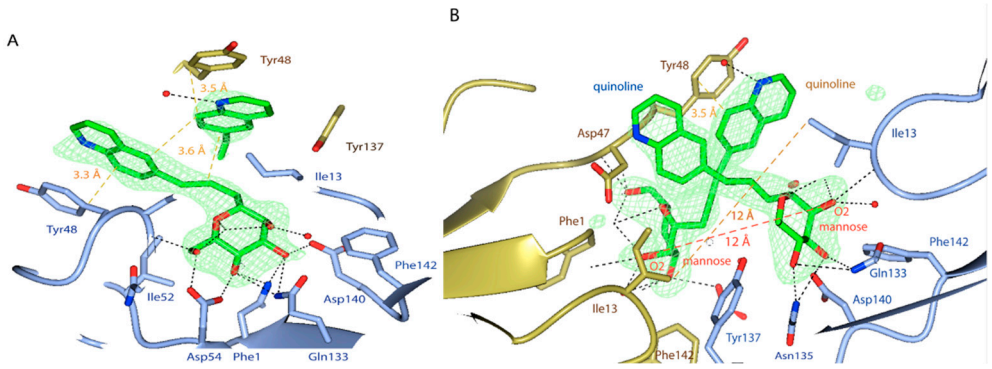

Figure 2. (**A**) Binding mode of quinoline inhibitor **11** (resolution 3Å). (**B**) The different colors show two neighboring FimH molecules (gold and blue) in the crystal packing. The distances between O_2 of each mannose and between the two Ile13 side chains, were 12 A°. (Protein PDB entry 8BVD).

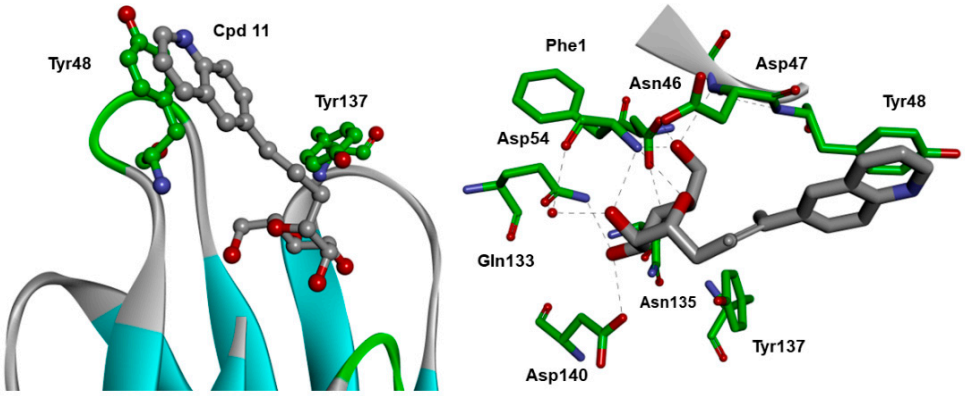

Figure 3. (**Left**) FimH lectin domain (amino acids 1-158) complexed with compound **11**. (**Right**) detailed molecular interactions of **11** with amino acids in the protein binding pocket of FimH: Phe1, Asp47, Gln133, Asp54, Asn135, Asp140 (PDB entry 8BVD). The carbon atom of the sugar ligand is grey and green for the FimH carbons.

Further Insights into the Design and Binding of Compound **20**

Given that the best compound **20** failed to crystallize with the FimH lectin domain, we tried to explain its improved potency using molecular dynamics (MD) simulations. The best low energy score was obtained from its docking within the FimH half-open tyrosine gate (−90.70 kcal/mol) (PDB 4AUY) (Figure 4). For comparison, the lowest FimH closed and open energy conformations were at −60.34 and −89.76 kcal/mol, respectively [48–51].

According to previous work [41], the ortho-biphenyl substituted C-linked mannopyranoside with K_D = 6.9 ± 5.7 nM had a higher affinity over the para-substituted analog (compound **18**, Table 1) with K_D = 17 ± 3.5 [41]. Previously published MD simulation with an ortho-substituted biphenyl derivative could nicely explain the origin of the better affinity observed with **20**. Indeed, the MD simulation allowed us to postulate that the higher affinity might originate from a π-stacking between the first phenyl ring of **20** with Tyr48, while the second ortho pyridyl moiety can interact with the hydroxyl group of Tyr137 through a hydrogen bond (2.70 A°). Thus, the MD simulation was instrumental in the replacement of the second phenyl group with a heterocyclic pyridyl moiety to improve the solubility as well as the affinity of ligand **20**.

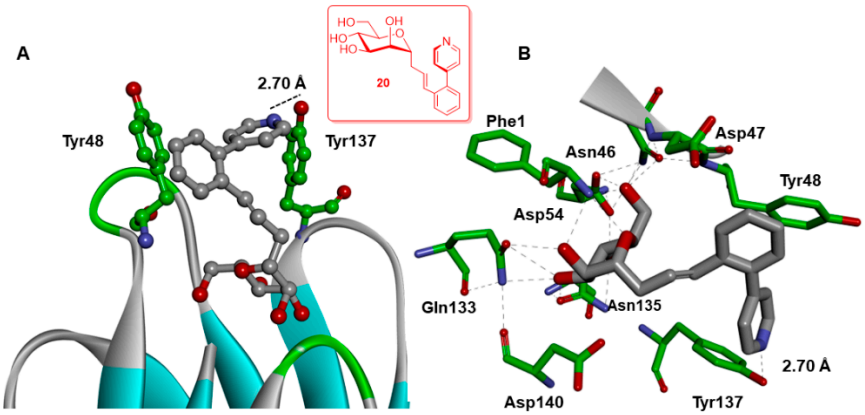

Figure 4. (**A**) Results of the Molecular Dynamics simulations in the docking of the *ortho*-biphenyl derivative **20** in the half-open FimH conformer (PDB entry 4AUY) [41]). (**B**) Detailed binding interactions between compound **20** within the *E. coli*-FimH lectin domain. Notice a potential hydrogen binding between the pyridine moiety and Tyr137. Colors of atoms are as in Figure 3.

2.5. Mannosides Do Not Affect Bacterial Growth, Cell Viability, and Antibiotic Activities

To test whether the above mannoside derivatives could exert bactericidal and/or cytotoxic activities, bacterial growth and cell viability assays were undertaken in the presence of each mannoside at different concentrations. Natural D-mannose (D-Man) was included as control. As shown in Figure 5, bacteria grown in the presence of mannoside analogs showed similar growth rates compared to bacteria grown in LB (Luria–Bertani) medium that represents the positive control for bacterial replication. Moreover, no cytotoxic effect was recorded for urinary bladder cell line 5637 (HTB-9 cell) monolayers [48,52], as measured by the MTT test (Figure 6). Since D-mannose can serve as nutrient replacement for *E. coli* when there is a shortage of D-glucose, we tested whether these new derivatives could be used as carbon sources as well [5]. To further this aim, bacteria were cultured in LB medium for 12 h and then diluted to 1.5×10^7 colony forming unit/mL (CFU/mL) in PBS buffer. Bacteria were incubated for an additional 24 h in the absence and in the presence of different mannosides and the number of viable bacteria was assessed by CFU/mL counting. Results show no statistically significant differences in the number of mannoside-treated bacteria compared to non-treated control (Figure 7). Conversely, the number of bacteria increased significantly in the presence of D-mannose, at both concentrations tested (500 μM and 83 mM) (Figure 7) [5]. The results indicated that the synthetic mannoside antagonists did not enter into the metabolic cycle of the bacterial cells to support their growth even in the absence of any other carbon sources. Differently, D-mannose as a natural sugar molecule is metabolized by bacteria, thereby maintaining bacterial replication [5]. Since carbohydrates can influence the activity of conventional antibiotics, the activity of different classes of antibiotics such as ampicillin (AMP 30 μg/mL), streptomycin (SM 50 μg/mL), and gentamycin (GM 50 μg/mL) in the presence of the synthetic mannoside analogs was evaluated. A broth-dilution test showed no differences in bacterial susceptibility, irrespectively in the presence of *C*-mannoside antagonists (Figure 8).

Altogether these results demonstrate the lack of toxicity of the synthetic mannoside derivatives toward both bacteria and eukaryotic cells. Moreover, these molecules are not used for bacterial metabolism and, unlike natural D-mannose, do not favor bacterial replication.

2.6. C-Mannoside Antagonists Are Effective in Decreasing Bacterial Adhesion to Human Bladder Epithelial Cells

To evaluate the efficacy of the synthetic mannoside antagonists to inhibit the ability of CFT073 strain to adhere to epithelial cells, an in vitro adhesion assay was performed. For this purpose, equal amounts of strain CFT073 strain were inoculated in PBS supplemented with different concentrations of each mannoside at final concentrations of 100, 500 μM, and 1 mM and incubated for 3h under static conditions. Bacterial inoculation was used to infect

cell line 5637 (HTB-9 cell) monolayers at a multiplicity of infection (MOI) of 10. At 2.5 h post-infection, the number of cell-associated bacteria was calculated by CFU/mL counting (Figure 9). No significant inhibition of bacterial adhesion to bladder cells was obtained using mannoside inhibitors at 100 µM. Conversely, a significant reduction (more than 1 log) in the number of adherent bacteria was observed by increasing the concentration of the mannosides to 500 µM in comparison to non-treated bacteria (Figure 10). The same extent of reduction in bacterial adhesion to bladder cells was obtained by increasing mannosides concentration to 1 mM, thereby showing a dose-dependent effect. Interestingly, among the mannosides studied, the quinoline analog **11**, having an IC_{50} of 3.17 nM, was the most efficient at reducing FimH-mediated bacterial adherence (Figures 9 and 10). On the other hand, compound **23** (MeMan) was the less efficient; however, it achieved the same extent of bacterial adhesion inhibition of natural D-mannose but at a 164-fold lower concentration. These results nicely confirmed previous observations from the control reference compounds **21**, **23**, and D-mannose [46]. To appraise qualitatively the reduction of bacterial adhesion, parallel infected cells were fixed, and Giemsa stained. As shown in Figure 10, no macroscopic differences in the shape, integrity, adhesiveness, cytoplasmic vacuolization, proliferation, or cytotoxic effects were observed in HTB-9 cell monolayers incubated with the synthesized mannosides, in line with the results of the MTT assay [5]. Overall, these results revealed that these synthetic inhibitors finely mimic the interaction between FimH and its natural receptor, thereby significantly decreasing the adhesion of strain CFT073 to bladder cells.

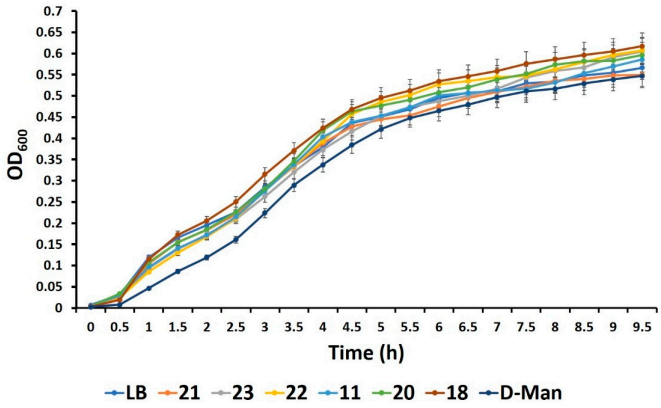

Figure 5. Bacterial growth is not affected by mannoside antagonists. Strain CFT073 was grown in LB medium supplemented with each mannoside derivative at a final concentration of 500 µM. Natural D-mannose (D-Man) at equal concentration to the mannosides was used as control. LB supplemented with DMSO (LB) was included as growth control. Bacterial cultures were incubated in a 96-well plate at 37 °C over a period of 10 h and the OD_{600} reads were determined every 30 min.

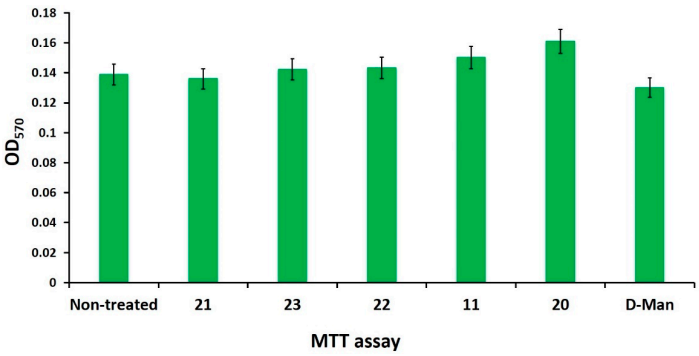

Figure 6. Mannoside antagonists do not alter the viability of urinary bladder cell line 5637 (HTB-9 cell). Cell monolayers were incubated with RPMI medium supplemented or not (non-treated) with

mannoside molecules and natural D-Man at a final concentration of 500 µM. Cell viability was assessed by the MTT assay by measuring the OD_{570}. Bars represent the means ± SDs of three experiments carried out in duplicate. *p* values were evaluated by one-way ANOVA; $p > 0.05$.

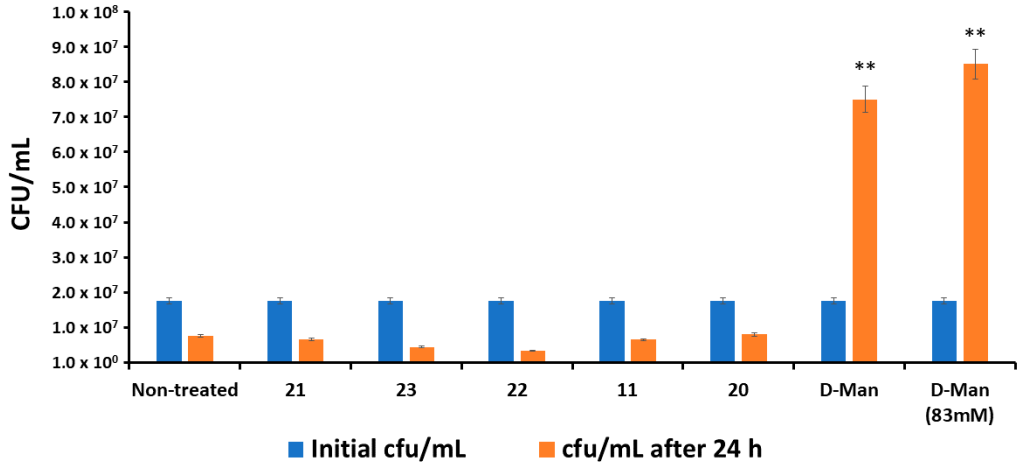

Figure 7. Only natural D-mannose (D-Man) supports the growth of strain CFT073. An initial inoculum of ~1.5 × 10^7 CFU/mL of strain CFT073 (blue bars) was incubated in PBS in the presence or absence (non-treated) of mannoside molecules at a final concentration of 500 µM for 24 h at 37 °C (orange bars). Natural D-mannose was added also at 83 mM. Bacterial CFU/mL were determined at endpoints. Bars represent the means ± SDs of two experiments carried out in duplicate. *p* values were evaluated by one-way ANOVA; ** $p \leq 0.01$.

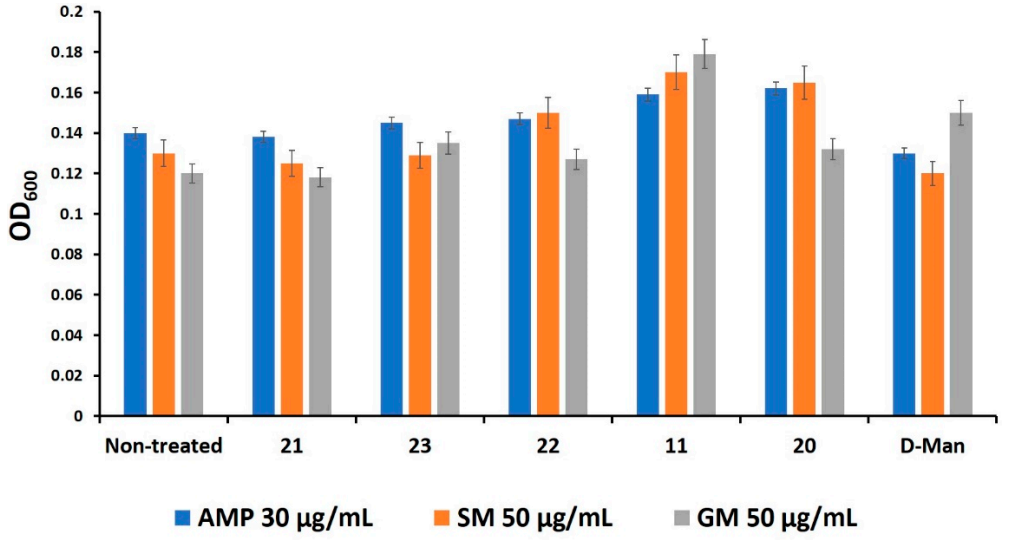

Figure 8. Mannoside antagonists do not affect antibiotic activity. The antibiotic susceptibility of strain CFT073 was assessed in the presence or absence (non-treated) of 500 µM mannosides and natural D-Man by broth-dilution assay. Bars represent the means ± SDs of two experiments carried out in duplicate. *p* values were evaluated by one-way ANOVA; $p > 0.05$.

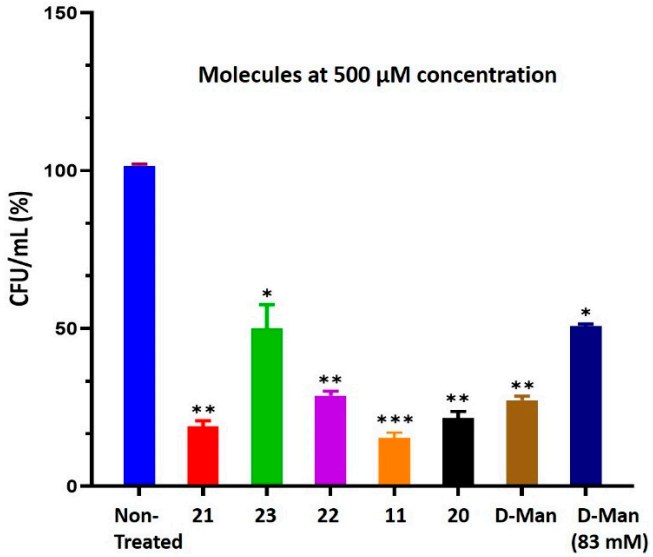

Figure 9. Mannoside antagonists efficiently inhibit bacterial adhesion to bladder cells. Bacteria were pre-incubated or not (non-treated) with mannose molecules at a final concentration of 500 µM. One mL of inoculation was used to infect HTB-9 cells at a MOI of 10. The total number of adherent bacteria was determined after 2.5 h of incubation and expressed as a percentage of CFU/mL (%) relative to the non-treated bacteria considered as 100%. Data represent the means ± SDs of three independent experiments performed in triplicate. p values were evaluated by one-way ANOVA; * $p < 0.05$, ** $p < 0.01$, *** $p < 0.001$.

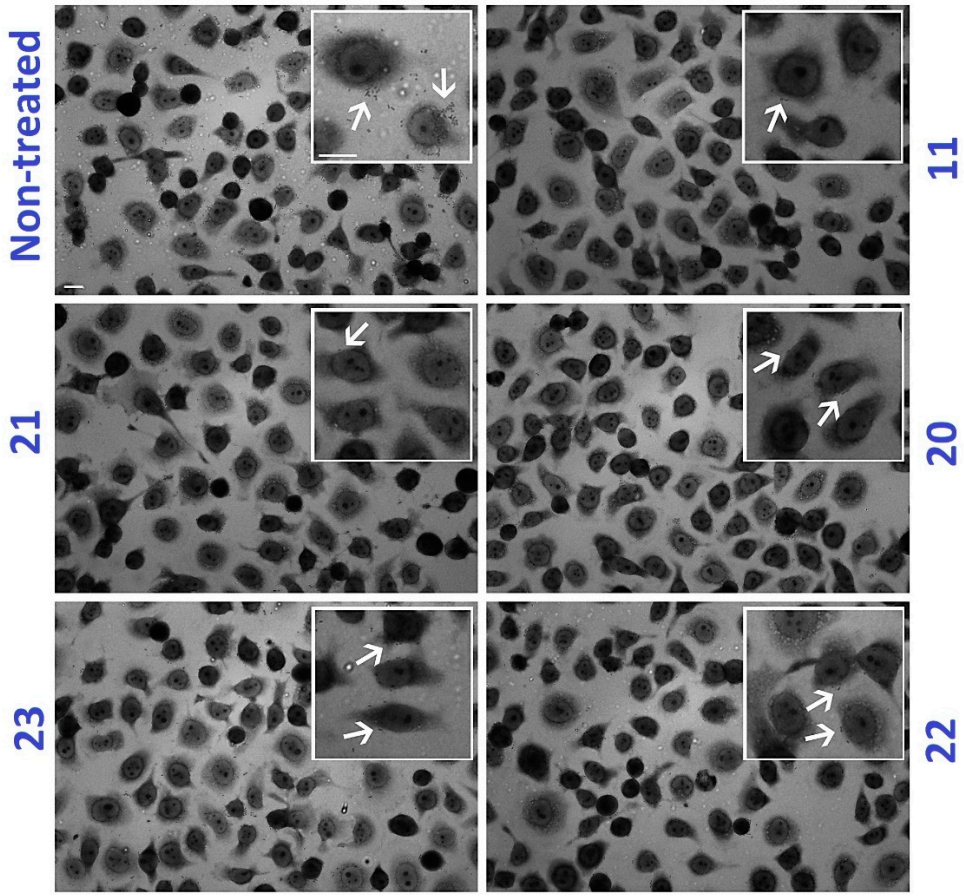

Figure 10. Mannoside antagonists **11**, **20**–**23** efficiently inhibit bacterial adhesion to bladder cells without adverse side effects. HTB-9 cell monolayers incubated with 500 µM mannosides were

Giemsa-stained after 2.5 h cell incubation. Representative images of three independent experiments are shown. Scale bar, 10 µm. Images were recorded with the 40× objective using a Leica DM5000B microscope and processed using the Leica Application Suite 2.7.0.R1 software (Leica). Arrows show the adherent bacteria.

3. Materials and Methods

3.1. General Information

Nuclear magnetic resonance (NMR) spectra were recorded on Varian Geminin 300 MHz or Innova 600 MHz spectrometer. Chemical shifts are reported in parts per million (ppm) (δ) relative to $CDCl_3$ (δ 7.27 and 77.23 ppm for ^{1}H- and ^{13}C-NMR, respectively) or relative to the signal of CD_3OD (δ. 3.31 and 4.8 ppm for ^{1}H- and 49.7 ppm for ^{13}C-NMR, respectively). Where necessary, DEPT, APT, and two-dimensional 1H-1H COSY and HSQC experiments were performed for complete signal assignments. Coupling constants (J) are reported in Hertz (Hz). Signal multiplicities are used as singlet (s), doublet (d), doublet of doublet (dd), triplet (t), multiplet (m). Accurate mass measurements were performed on a LC-MSD-Tof instrument from Agilent technologies in positive electrospray with protonated ions $[M + H]^+$; sodium adducts $[M + Na]^+$ and $[M + NH_4]^+$ were used for empirical formula confirmation. Flash chromatography was performed using Merck silica gel 60 (40–63 µm). TLC was performed on Kiesel gel 60 F254 plates from Merck. Detection was carried out under UV light or by spraying with 20% ethanolic sulfuric acid or molybdate solution followed by heating. Optical rotations were measured with a JASCO P-1010 polarimeter. Melting points were measured on a Fisher Jones apparatus and are uncorrected. Purification of some compounds were done by semi-preparative HPLC (Agilent, Santa Clara, CA, USA). All eluents contained 0.1% formic acid and flow rate was set to 5 mL/min. Solvents were dried by distillation from drying agents as follows: DMF (Barium oxide), CH_2Cl_2 (P_2O_5), Et_3N and pyridine (CaH_2), MeOH was stored over 4A molecular sieves. Some aryl iodides were synthesized according to literature procedures [53–55]: 2-iodophenyl acetate, 4-iodophenyl acetate, 4-iodobenzyl acetate and methyl 4-iodobenzoate. Compound **9** and **18** were prepared as previously published [30].

3.2. Synthetic Methods and Analytic Data of Compounds

3.2.1. General procedure for Heck Coupling of Protected C-Mannopyranosides **2–10**

To a solution of mannopyranosides **1** [40] in degassed anhydrous DMF, were added the various iodoaryl derivatives (2 equiv.), 10% palladium(II) acetate, tetrabutylammonium bromide (1 equiv.), and sodium bicarbonate (3 equiv.). The reaction mixture was heated at 85 °C under N_2. The course of the reactions was followed by TLC. The solution was evaporated under reduced pressure and the residue was purified by flash column chromatography on silica gel (from 0 to 425% AcOEt-Hexanes).

Compound **2**: 40 mg, 0.053 mmol, 66%, $[\alpha]^{20}_D = -9.13$ (c = 0.5, $CHCl_3$). *Rf* = 0.29 (Hexane/EtOAc, 5.5: 4.5), m.p: 149–150 °C. ^{1}H-NMR (600 MHz, $CDCl_3$): δ ppm 8.8–7.19 (m, 26H, H-arom), 6.75 (d, 1H, $J_{2',3'}$ = 15.8 Hz, CH=CH-), 6.46–6.36 (m, 1H, CH=CH-), 5.98–5.88 (m, 2H, H-4, H-3), 5.27 (dd, 1H, $J_{1,2}$ = J2, 3 = 2.7 Hz, H-2), 4.75 (dd, 1H, $J_{6a,6b}$ = 12.0 Hz, J5, 6a = 6.9 Hz, H-6a), 4.50 (dd, 1H, $J_{6a,6b}$ = 12.0 Hz, $J_{5,6b}$ = 2.6 Hz, H-6b), 4.56–4.52 (m, 1H, H-1), 4.50–4.47 (m, 1H, H-5), 3.05–2.96 (m, 1H, H-1'a), 2.85–2.75 (m, 1H, H-1'b). ^{13}CNMR (151 MHz, $CDCl_3$): δ ppm, 166.2, 165.9, 165.6, 165.4 (4×CO), 150.1, 147.9, 135.89, 135.1, 133.5, 133.4, 132.9, 129.8, 129.6, 129.5, 128.59, 128.5, 128.2, 127.0, 121.3 (Carom, C-3', C-2'), 74.2 (C-1), 71.2 (C-5), 71.1 (C-4), 69.6 (C-3), 68.0 (C-2), 62.9 (C-6), 33.1 (C-1'). ESI^+-HRMS: $[M + H]^+$ calcd for $C_{46}H_{37}NO_9$ + H+: 748.2541; found, 748.2479.

Compound **3**: 44.6 mg, 0.064 mmol, 80 %. $[\alpha]^{20}_D = -28.86$ (c = 0.2, $CHCl_3$). R_f = 0.23 (Hexane/EtOAc, 1.8:1.2). ^{1}H-NMR (600 MHz, $CDCl_3$): δ ppm 8.44 (d, 1H, $^4J_{H\text{-}H}$ = 2.2 Hz, H-arom), 8.36 (dd, 1H, $^3J_{H\text{-}H}$ = 4.7 Hz, $^4J_{H\text{-}H}$ = 1.5 Hz, H-arom), 7.91–7.21 (m, 21H, H-arom), 7.11–6.93 (m, 1H, H-arom), 6.51 (d, 1H, $J_{2',3'}$ = 16 Hz, CH=CH-Py), 6.24 (m, 1H, $J_{2',3'}$ = 16.3 Hz, $J_{2',H1'a}$ = 13.4 Hz, $J_{2',H1'b}$ = 5.8 Hz C<u>H</u>=CH-Py), 6.02 (dd, 1H, $J_{3,4} = J_{4,5}$ = 8.3 Hz, H-4), 5.81 (dd,

1H, $J_{2,3}$ = 3.1 Hz, $J_{3,4}$ = 8.6 Hz, H-3), 5.63 (dd, 1H, $J_{1,2}$ = $J_{2,\ 3}$ = 3.4 Hz, H-2), 4.68 (dd, 1H, $J_{6a,6b}$ = 12.0 Hz, $J_{5,6a}$ = 6.7 Hz, H-6a), 4.52 (dd, 1H, $J_{6a,6b}$ = 12. Hz, $J_{5,6b}$ = 3.2 Hz, H-6b), 4.46–4.41 (m, 1H, H-1), 4.38–4.35 (m, 1H, H-5), 2.94–2.82 (m, 1H, H-1′a), 2.74–2.68 (m, 1H, H-1′b). ^{13}CNMR (151 MHz, $CDCl_3$): δ ppm, 166.2, 165.6, 165.6, 165.4 (4 × CO), 148.4, 148.2, 133.5, 133.4, 133.0, 132.4, 129.6, 128.9, 128.5, 126.7, 123.5 (Carom, C-3′, C-2′), 74.1 (C-1), 71.2 (C-5), 71.1 (C-2), 69.4 (C-4), 67.80 (C-3), 62.7 (C-6), 33.2 (C-1′). ESI$^+$-HRMS: $[M + H]^+$ calcd for $C_{42}H_{35}NO_9$ + H+: 698.2385; found, 698.4013.

Compound **4**:115 mg, 0.152 mmol, 80% yield. $[\alpha]^{20}_D$ = −9.92 (c = 0.5, $CHCl_3$). R_f = 0.17 (Hexane/EtOAc, 2:1). ^{1}H-NMR (300 MHz, $CDCl_3$): δ, 8.21–7.00 (m, 24H, H-arom), 6.67 (d, 1H, $J_{2',3'}$ = 15.9 Hz, CH=C<u>H</u>Ph), 6.39–6.2 (m, 1H, C<u>H</u>=CHPh), 6.00 (dd, 1H, $J_{3,4}$ =$J_{4,5}$ = 8.5 Hz, H-4), 5.91 (dd, 1H, $J_{2,3}$ = 3.1 Hz, $J_{3,4}$ = 8.9 Hz, H-3), 5.74 (dd, 1H $J_{1,2}$ = $J_{2,3}$ = 3.1 Hz, H-2), 4.66 (m, 2H, H-6a, H-6b), 4.74 (dd, 1H, $J_{6a,\ 6b}$ = 12 Hz, $J_{5,\ 6a}$ = 6.5 Hz, H-6a), 4.62 (dd, 1H, $J_{5,\ 6b}$ = 12 Hz, $J_{6a,\ 6b}$ = 2.8 Hz, H-6b), 4.59–4.36 (m, 2H, H-1, H-5), 3.09–2.92 (m, 1H, H-1′a), 2.85–2.78 (m, 1H, H-1′b), 2.37 (s,3H, Ac). ^{13}C-NMR (75 MHz, $CDCl_3$): δ 169.3, 166.2, 165.6, 165.4, 147.5 (5 × CO), 135.5, 133.4, 133.0, 129.8, 129.6, 129.5, 129.0, 128.4, 128.2, 126.7, 126.1, 122.5 (Carom, C-3′, C-2′), 74.4 (C-1), 71,4 (C-5), 71.0 (C-4), 69.7 (C-3), 67.8 (C-2), 62.8 (C-6), 33.23 (C-1′) and 21.1 (Ac). ESI$^+$-HRMS: $[M + H]^+$ calcd for C_{45} H_{39} O_{11}, 755.2487; found, 755.2469.

Compound **5**: 49 mg, 0.064 mmol 80% yield. $[\alpha]^{20}_D$ = −16.63 (c = 0.5, $CHCl_3$)). R_f = 0.22 (Hexane/Toluene/EtOAc, 71: 24: 5). ^{1}H-NMR (300 MHz, $CDCl_3$): δ, 8.14–7.29 (m, 22H, H-arom), 6.98 (dd, 1H, $^3J_{H\text{-}H}$ = 9.0 Hz, $^4J_{H\text{-}H}$ = 2.4 Hz, H-arom), 6.61 (d, 1H, $J_{2',3'}$ = 15.9 Hz, CH=C<u>H</u>Ph), 6.32–6.17 (m, 1H, C<u>H</u>=CHPh), 5.95 (dd, 1H, $J_{3,4}$ =$J_{4,5}$ = 8.8 Hz, H-4), 5.90 (dd, 1H, $J_{2,3}$ = 3.0 Hz, $J_{3,4}$ = 8.8 Hz, H-3), 5.74 (dd, 1H $J_{1,2}$ = $J_{2,3}$ = 3.1 Hz, H-2), 4.72 (dd, 1H, $J_{6a,6b}$ = 12 Hz, $J_{5,6a}$ = 6.5 Hz, H-6a), 4.62 (dd, 1H, $J_{6a,6b}$ = 12.1 Hz, $J_{5,6b}$ = 2.8 Hz, H-6b), 4.56–3.36 (m, 2H, H-1, H-5), 3.05–2.87 (m, 1H, H-1′a), 2.83–2.79 (m, 1H, H-1′b), 2.32 (s, 3H, Ac). ^{13}C-NMR (75 MHz, $CDCl_3$): δ 169.3, 166.3, 165.6, 165.4, 147.5 (5 × CO), 135.4, 133.3, 133.0, 129.8, 129.5, 129.0, 128.4, 126.7, 126.1, 122.5 (Carom, C-3′, C-2′), 74.4 (C-1), 71,4 (C-5), 71.0 (C-4), 69.7 (C-3), 67.8 (C-2), 62.8 (C-6), 33.23 (C-1′) and 21.0 (Ac). ESI$^+$-HRMS: $[M + H]^+$ calcd for $C_{45}H_{39}O_{11}$, 755.2487; found, 755.2453.

Compound **6**: 52 mg, 0.067 mmol, 90% yield. $[\alpha]^{20}_D$ = −8.3 (c = 0.5, $CHCl_3$). R_f = 0.25 (Hexane/ EtOAc, 3:1). ^{1}H-NMR (300 MHz, $CDCl_3$): δ, 8.16.7.12 (m, 24H, H-arom), 6.63 (d, 1H, $J_{2',3'}$ = 15.8 Hz, CH=C<u>H</u>Ph), 6.49–6.21 (m, 1H, C<u>H</u>=CHPh), 6.08–5.84 (m, 2H, H-4, H-3), 5.75 (dd, 1H $J_{1,2}$ = $J_{2,3}$ = 2.9 Hz, H-2), 5.11 (s, 2H, C<u>H$_2$</u>Ph), 4.72 (dd,1H, $J_{6a,6b}$ = 11.9 Hz, $J_{5,6a}$ = 6.3 Hz, H-6a), 4.63 (dd, 1H, $J_{6a,6b}$ = 11.9 Hz, $J_{5,6b}$ = 2.6 Hz, H-6b), 4.57–4.39 (m, 2H, H-1, H-5), 3.01–2.93 (m, 1H, H-1′a), 2.84–2.77 (m, 1H, H-1′b), 2.84–2.77 (s, 3H, Ac). ^{13}C-NMR (75 MHz, $CDCl_3$): δ 166.2, 165.6, 165.6, 165.4, 137.6 (5 × CO), 134.9, 133.4, 133.0, 132.8, 129.8, 129.5, 128.9, 128.5, 126.3, 124.7 (Carom, C-3′, C-2′), 74.5 (C-1), 71,2 (C-5), 70.9 (C-4), 69.7 (C-3), 67.8 (C-2), 66.1 (<u>C</u>H$_2$Ph), 63.0 (C-6), 29.6 (C-1′) and 21.0 (Ac). ESI$^+$-HRMS: $[M+NH_4]^+$ calcd for $C_{46}H_{44}NO_{11}$, 786.2909; found, 786.2919.

Compound **7**: 194 mg, 0.237, 73% yield. $[\alpha]^{20}_D$ = −16.6 (c = 0.3, $_{CHCl3}$). *Rf* = 0.18 (Hexane/EtOAc, 3:1). ^{1}H-NMR (300 MHz, $CDCl_3$): δ, 8.11–7.08 (m, 24H, H-arom), 6.65 (d, 1H, $J_{2',3'}$ = 15.9 Hz, CH=CHPh), 6.45–6.35 (m, 1H, CH=CHPh), 6.01–5.88 (m, 2H, H-4, H-3), 5.75 (dd, 1H, $J_{1,2}$ = 3.9 Hz, $J_{2,3}$ = 7.3 Hz, H-2), 4.78 (dd, 1H, $J_{6a,6b}$ = 12.0 Hz, $J_{5,6a}$ = 6.7 Hz, H-6a), 4.63 (dd, 1H, $J_{6a,6b}$ = 12 Hz, $J_{5,6b}$ = 2.8 Hz, H-6b), 4.58–4.42 (m, 2H, H-1, H-5), 3.93 (s, 3H, COOMe), 3.03–2.93 (m, 1H, H-1′a), 2.92.-2.71 (m, 1H, H-1′b). ^{13}C-NMR (75 MHz, $CDCl_3$): δ 166.8, 166.2, 165.7, 165.4, 141.4 (5 × CO), 133.4, 133.1, 132.4, 129.7, 129.6, 128.9, 128.5, 128.3, 127.1, 126.0 (Carom, C-3′, C-2′), 74.1 (C-1), 71.3 (C-5), 71.2 (C-4), 69.6 (C-3), 67.9 (C-2), 62.8 (C-6), 51.9 (COOMe), 33.1 (C-1′). ESI$^+$-HRMS: $[M + H]^+$ calcd for $C_{45}H_{39}O_{11}$, 755.2487; found, 755.2493.

Compound **8**: 158 mg, 88% yield. $[\alpha]^{20}$D = −6.12 (c = 0.5, $CHCl_3$). R_f = 0.27 (Hexane/EtOAc, 3:1)^{1}H-NMR (300 MHz, $CDCl_3$): δ, 8.09–7.31 (m, 24H, H-arom), 6.65 (d, 1H, $J_{2',3'}$ = 15.9 Hz, CH=C<u>H</u>Ph), 6.44 (m, 1H, C<u>H</u>=CHPh), 5.90 (m, 2H, H-4, H-3), 5.74 (dd, 1H $J_{1,2}$ =3.7, Hz, $J_{2,3}$ = 2.4 Hz, H-2), 4.86 (dd, 1H, $J_{6a,6b}$ = 12 Hz, $J_{5,6a}$ = 7.2 Hz, H-6a), 4.63–4.44 (m, 3H, H-6b, H-1, H-5), 3.12–2.98 (m, 1H, H-1′a), 2.76–2.85 (m, 1H, H-1′b). ^{13}C-NMR

(75 MHz, $CDCl_3$): δ 166.2, 165.6, 165.4, 164.7 (4 × CO), 146.7, 143.3, (Carom-q),133.5, 133.1, 131.3, 129.8, 128.9, 128.3, 126.5, 123.6, (Carom, C-3′, C-2′), 73.4 (C-1), 71.4 (C-5), 71.0 (C-4), 69.4 (C-3), 68.2 (C-2), 62.6 (C-6), 33. 3 (C-1′). ESI^+-HRMS: $[M + Na]^+$ calcd for $C_{45}H_{35}NO_{11}$, 764.2102; found, 764.2157.

Compound **10**: This compound was synthesized according to general procedure A. 56 mg, 0.072 mmol, 90% yield, $[\alpha]^{20}_D = -14.16$ (c = 0. 39, $CHCl_3$). *Rf* = 0.27. (Hexane/EtOAc, 9:3). ^{1}H-NMR (300 MHz, $CDCl_3$): δ, 8.69 (d, 1H, $^3J_{H\text{-}H}$ = 5.6 Hz), 8.10–7.23 (m, 23H, H-arom), 6.56 (d, 1H, $J_{2',3'}$ = 15.7 Hz, CH=C<u>H</u>Ph), 6.33–6.12 (m, 1H, C<u>H</u>=CHPh), 6.01 (dd, 1H, $J_{3,4}$ = 12 Hz, $J_{4,5}$ = 9.0 Hz, H-4), 5.92 (dd, 1H, $J_{2,3}$ = 3.1 Hz, $J_{3,4}$ = 9.0 Hz, H-3), 5.15 (dd, 1H $J_{1,2} = J_{2,3}$ = 3.1 Hz, H-2), 3.93–3.90 (m, 1H, H-1), 4.72 (dd, 1H, $J_{6a,6b}$ = 12.1, Hz, $J_{5,6a}$ = 6 Hz, H-6a), 4.58–4.41 (m, 2H, H-5, H-1), 3.09–2.98 (m, 1H, H-1′a), 2.93–2.76 (m, 1H, H-1′b). ^{13}C-NMR (75 MHz, $CDCl_3$): δ 166.2, 166.6, 165.6, 165.4, (4 × CO), 136.8, 133.3, 133.0, 132.8, 132.2, 129.7, 128.5, 128.9, 128.4, 127.5, 127.3, 127.1, 123.3 (Carom- C-3′,C-2′), (Carom), 127.5 (Carom, C-2′), 127.3, 127.1 (Carom), 74.5 (C-1), 71,3 (C-5), 70.9 (C-4), 69.7 (C-3), 67.8 (C-2), 62.9 (C-6), 32.9 (C-1′). ESI^+-HRMS: $[M + NH_4]^+$: calcd for $C_{43}H_{39}BrNO_9$, 794.1792; found, 794.1770

3.2.2. General Procedure for De-O-Benzoylation

Compounds **11–18** and **20** were deprotected by treatment with 1M ammonia in methanol at room temperature for 36 h. Removal of solvent under vacuum afforded the crude residues which were purified by column chromatography (MeCN/MeOH, 9.5/0.5) and the compounds (11, 13, 15) were purified by semi-preparative HPLC (A: H_2O + 0.1% trifluoroacetic acid, B: ACN + 0.1% trifluoroacetic acid, 5 mL/min).

Compound **11**: 15 mg, 0.045 mmol, 85% yield. $[\alpha]^{20}_D$ = +41.3 (*c* = 0.1, CH_3OH). ^{1}H-NMR (600 MHz, CD_3OD): δ ppm 8.87 (dd, 1H, $^3J_{H\text{-}H}$ = 4.4 Hz, $^4J_{H\text{-}H}$ = 1.6 Hz, H-arom), 8.33 (dd, 1H, $^3J_{H\text{-}H}$ = 8.4 Hz, $^4J_{H\text{-}H}$ = 1.6 Hz, H-arom), 7.97 (d, 2H, $^3J_{H\text{-}H}$ = 1.1 Hz, H-arom), 7.84 (s, 1H, H-arom), 7.52 (dd, 1H, $^3J_{H\text{-}H}$ = 8.3 Hz, $^4J_{H\text{-}H}$ = 4.4 Hz, H-arom), 6.75 (d, 1H, $J_{2',3'}$ = 16.0 Hz, CH=C<u>H</u>-), 6.65–6.48 (m, 1H, C<u>H</u>=CH-), 4.07 (ddd, 1H, $J_{1,2}$ = 2.7 Hz, $J_{1,H1'a}$ = 8.7 Hz, $J_{1,\,H1'b}$ = 6.0 Hz, H-1), 3.84–3.65 (m, 5H, H-4, H-3, H-2, H-6a H-6b), 3.64–3.55 (m, 1H, H-5), 2.84–2.69 (m, 1H, H-1′a), 2.68–2.51 (m, 1H, H-1′b). ^{13}C-NMR (151 MHz, CD_3OD): δ ppm: 149.2, 146.8, 136.9, (Carom-q), 136.4, 131.1, 128.4, 128.2, 127.6, 127.4, 125.2, 121.4, (Carom, C-3′, C-2′), 76.6 (C-1), 75,0 (C-5), 71.3 (C-4), 70.7 (C-3), 68.1 (C-2), 61.6 (C-6), 32.6 (C-1′). ESI^+-HRMS: $[M + H]^+$ calcd for $C_{18}H_{21}NO_5$, 332.1492; found, 332.1515.

Compound **12**: 15 mg, 0.053 mmol, 84% yield. $[\alpha]^{20}_D$ = +27.8 (*c* = 0.1, CH_3OH). ^{1}H-NMR (300 MHz, CD_3OD): δ ppm 8.53 (s, 1H, H-arom), 8.38 (d, 1H, $^3J_{H\text{-}H}$ = 3.8 Hz, H-arom), 7.94 (dd, 1H, $^3J_{H\text{-}H}$ = 3.5 Hz, $^4J_{H\text{-}H}$ = 1.8 Hz, H-arom), 7.42- (dd, 1H, $^3J_{H\text{-}H}$ = 8.0 Hz, $^4J_{H\text{-}H}$ = 4.9 Hz, H-arom), 6.60 (d, 1H, $J_{2',3'}$ = 16.0 Hz, CH=C<u>H</u>-Py), 6.50–6.41 (m, 1H, C<u>H</u>=CH-Py), 4.08 (ddd, 1H, $J_{1,2}$ = 2.7 Hz, $J_{1,H1'a}$ = 8.7 Hz, $J_{1,H1'b'}$ = 6 Hz, H-1) 3.91–3.65 (m, 5H, H-4, H-3, H-2, H-6a, H-6b), 3.62–3.57 (m, 1H, H-5), 2.81–2.69 (m, 1H, H-1′a), 2.62–2.51 (m, 1H, H-1′b). ^{13}C-NMR (75 MHz, CD_3OD): δ ppm: 146.9, 146.6, 133.6, 129.3, 128.2, 124.2, 121.1 (Carom, C-3′, C-2′), 76.8 (C-1), 74.1 (C-5), 70.7 (C-4), 70.7 (C-3), 67.5 (C-2), 61.4 (C-6), 32.5 (C-1′). ESI^+-HRMS: $[M + H]^+$: calcd for $C_{14}H_{19}NO_5$, 282.1336; found, 282.1331.

Compound **13**: 38 mg, 0.128 mmol, 85% yield. $[\alpha]^{20}_D$ = +8.54 (c = 0.2, CH_3OH). ^{1}H-NMR (300 MHz, CD_3OD): δ, 7.38 (dd, 1H, $^3J_{H\text{-}H}$ = 8.3 Hz, $^4J_{H\text{-}H}$ = 1.3 Hz, H-arom), 7.03 (td, 1H, $^3J_{H\text{-}H}$ = 7.7 Hz, $^4J_{H\text{-}H}$ = 1.6 Hz, H-arom), 6.76 (m, 3H, H-arom, CH=C<u>H</u>Ph), 6.31–6.21 (m, 1H, C<u>H</u>=CHPh), 4.06–3.96 (m, 1H, H-1), 3.89–3.61 (m, 5H, H-4, H-3, H-6a, H-6b, H-2), 3.56 (ddd, 1H, $J_{4,5}$ = 8.5 Hz, $J_{5,6a}$ = 5.4 Hz, $J_{5,6b}$ = 2.9 Hz, H-5), 3.01 (s, 1H, PhO<u>H</u>), 2.66 (ddd, 1H, 1H, $J_{H1'a,\,H1'b}$ = 14.7 Hz, $J_{1,H1'a}$ = 1.4 Hz, $J_{1',2'}$ = 8.1 Hz, H-1′a), 2.54 (ddd, 1H, 1H, $J_{H1'a,H1'b}$ = 14.4 Hz, $J_{1,H1'b}$ = 3.9 Hz, $J_{H1'b,2'}$ = 10.6 Hz, H-1′b). ^{13}C-NMR (75 MHz, CD_3OD): δ 154.1 (C-PhOH), 127.5 (C-3′), 127.3, 126.2 (Carom-q), 122.0 (C-2′), 124.4, 118.9, 115.0 (Carom), 77.5 (C-1), 74,8 (C-5), 71.4 (C-4), 70.6 (C-3), 67.9 (C-2), 61.6 (C-6), 33.09 (C-1′). ESI^+-HRMS: $[M+Na]^+$: calcd for $C_{15}H_{20}NaO_6$, 319.1158; found, 319.1175.

Compound **14**: 16 mg, 0.054 mmol, 85% yield. $[\alpha]^{20}_{D}$ = +31 (c = 0.1, CH_3OH). ^{1}H-NMR (300 MHz, CD_3OD): δ, 7.23 (d, 2H, $^3J_{H-H}$ = 8.6 Hz, H-arom), 6.72 (d, 2H, $^3J_{H-H}$ = 8.6 Hz, H-arom), 6.42 (d, 1H, $J_{2',3'}$ = 15.7 Hz, CH=C<u>H</u>Ph), 6.14–6.04 (m, 1H, C<u>H</u>=CHPh),4.10–3.91 (m, 1H, H-1), 3.87–3.61 (m, 5H, H-4, H-3, H-6a, H-6b, H-2), 3.62–3.44 (m, 1H, H-5), 2.66–2.57 (m, 1H, H-1'a), 2.53–2.43 (m, 1H, H-1'b). ^{13}C-NMR (75 MHz, CD_3OD): δ 153.6 (C-PhOH), 131.7 (C-3'), 129.1, 126.9 (Carom-q), 122.6 (C-2'), 115.1 (Carom), 77.5 (C-1), 74,8 (C-5), 71.4 (C-4), 70.6 (C-3), 67.9 (C-2), 61.6 (C-6), 33.09 (C-1'). ESI$^+$-HRMS: $[M+Na]^+$: calcd for $C_{15}H_{20}NaO_6$, 319.1152; found, 319.1165.

Compound **15**: 16.2 mg, 0.052 mmol, 80% yield. $[\alpha]^{20}_{D}$ = +20 (c = 0.1, CH_3OH). ^{1}H-NMR (300 MHz, CD_3OD): δ, 7.38 (d, 2H, $^3J_{H-H}$ = 8.2 Hz, H-arom), 7.29 (d, 2H, $^3J_{H-H}$ = 8.2 Hz, H-arom), 6.52 (d, 1H, $J_{2',3'}$ = 15.9 Hz, CH=C<u>H</u>Ph), 6.39–6.24 (m, 1H, C<u>H</u>=CHPh),4.58 (s, 2H, C<u>H</u>$_2$Ph), 4.07–3.94 (m, 1H, H-1), 3.86–3.61 (m, 5H, H-4, H-3, H-6a, H-6b, H-2), 3.56 (ddd, 1H, $J_{4,5}$ = 8.5 Hz, $J_{5,6a}$ = 5.5 Hz, $J_{5,6b}$ = 3.0 Hz, H-5), 2.72–2.61 (m, 1H, H-1'a), 2.57–2.61 (m, 1H, H-1'b). ^{13}C-NMR (75 MHz, CD_3OD): δ 140.2,136.6 (Carom-q), 131.8, (C-3'), 126.8, 125.7 (Carom), 125.6, (C-2'), 77.2 (C-1), 74,9 (C-5), 71.2 (C-4), 70.7 (C-3), 68.0 (C-2), 63.5 (<u>C</u>H$_2$Ph), 61.6 (C-6), 32.4 (C-1'). ESI$^+$-HRMS: $[M+NH_4]^+$: calcd for $C_{16}H_{26}NO_6$, 328.1416; found, 328.1771.

Compound **16**: 16 mg, 0.047 mmol, 85% yield. $[\alpha]^{20}_{D}$ = +42.62 (c = 0.1, CH_3OH). ^{1}H-NMR (300 MHz, CD_3OD): δ, 7.95 (d, 2H, $^3J_{H-H}$ = 8.4 Hz, H-arom), 7.51 (d, 2H, $^3J_{H-H}$ = 8.4 Hz, H-arom), 6.64–6.44 (m, 2H, CH=C<u>H</u>Ph, C<u>H</u>=CHPh), 4.04 (ddd, 1H, $J_{1,2}$ = 6.0 Hz, $J_{1,1'a}$ = 8.7 Hz, $J_{1,1'b}$ = 2.7 Hz, H-1), 3.83 (dd, 1H, $J_{3,4}$ =6.1 Hz, $J_{4,5}$= 3.1 Hz, H-4,), 3.81–3.64 (m, 4H, H-3, H-6a, H-6b, H-2), 3.55 (ddd, 1H, $J_{4,5}$ = 9.9 Hz, $J_{5,6a}$ = 6.5 Hz, $J_{5,6b}$ = 3.8 Hz, H-5), 2.76–2.66 (m, 1H, H-1'a), 2.64–2.47 (m, 1H, Hb). ^{13}C-NMR (75 MHz, CD_3OD): δ 167.0 (<u>C</u>OOMe), 142.3 (Carom-q), 131.0 (C-3'), 129.4 (Carom-q), 128.2, 125.9 (C-2'), 77.1 (C-1), 75,2 (C-5), 70.9 (C-4), 70.7 (C-3), 67.8 (C-2), 61.5 (C-6), 51.4 (COO<u>Me</u>), 32.6 (C-1'). ESI$^+$-HRMS: $[M+Na]^+$: calcd for $C_{17}H_{22}NaO_7$, 361.1258; found, 361.1253.

Compound **17**: 16 mg, 0.049 mmol, 85% yield. $[\alpha]^{20}_{D}$ = +40.6 (c = 0.1, CH_3OH). ^{1}H-NMR (300 MHz, CD_3OD): δ, 8.19 (d, 2H, $^3J_{H-H}$ = 5 Hz, H-arom), 7.64 (d, 2H, $^3J_{H-H}$ = 4.9 Hz, H-arom), 6.95–6.45 (m, 2H, CH=C<u>H</u>Ph, C<u>H</u>=CHPh), 4.26–3.89 (m, 1H, H-1), 3.84–3.54 (m, 6H, H-4, H-3, H-6a, H-6b, H-2, H-5), 3.10–2.64 (m, 1H, H-1'a), 2.71–2.37 (m, 1H, H-1'b). ^{13}C-NMR (75 MHz, CD_3OD): δ 146.4, 144.3 (Carom-q), 132.1, 129.9, 126.2, 123.7 (Carom, C-3', C-2'), 76.5 (C-1), 74.9 (C-5), 71.1 (C-4), 76.5 (C-3), 67.9 (C-2), 61.2 (C-6), 32.4 (C-1'). ESI$^+$-HRMS: $[M+NH_4]^+$: calcd for $C_{15}H_{23}N_2O_7$, 343.15; found, 343.1512.

3.2.3. Synthesis of Compounds **19** and **20** by Suzuki Reaction

To a solution of compound **10** (40 mg, 0.051 mmol) in degassed (N_2) dioxane-water (5:1) were added 4-piridinylboronicacid (10 mg, 2 equiv.), 15% Pd_2Cl_2 $(PPh_3)_2$ ferrocene, and cesium carbonate (48 mg, 3 equiv.). The reaction mixture was heated at 80 ^{0}C. The reaction was followed by TLC. The solution was evaporated under reduced pressure and the residue was purified by flash column chromatography on silica gel (6:4 Hexane/EtOAc) to afford compound **19** as colorless oil. 22 mg, 0.028 mmol, 55%, $[\alpha]^{20}_{D}$ = −10.7 (c = 0. 4, $CHCl_3$). *Rf* = 0.17 (Hexane/EtOAc, 6:4). ^{1}H-NMR (300 MHz, $CDCl_3$): δ, 8.69 (d, 1H, H-arom), 8.06.7.23 (m, 27H, H-arom), 6.56 (d, 1H, $J_{2',3'}$ = 15.6 Hz, CH=C<u>H</u>Ph), 6.28 (ddd, 1H, $J_{1'a,2'}$ = $J_{1'b}$, 2'=6.9 Hz, $J_{2',3'}$ = 15.6 Hz, C<u>H</u>=CHPh), 6.01 (dd, 1H, $J_{3,4}$ = $J_{4,5}$ = 8.6 Hz, H-4), 5.92 (dd, 1H, $J_{2,3}$ = 3.3 Hz, $J_{3,4}$ = 9.0 Hz, H-3), 5.72 (dd, 1H $J_{1,2}$ = $J_{2,3}$ = 3.2 Hz, H-2), 4.71 (dd, 1H, $J_{6a,6b}$ = 12.1 Hz, $J_{5,6a}$ = 5.9 Hz, H-6a), 4.62 (dd, 1H, $J_{6a,6b}$ = 12.2 Hz, $J_{5,6b}$ = 2.9 Hz, H-6a), 4.52–4.44 (m, 1H, H-1), 4.41–4.34 (m, 1H, H-5), 2.94–2.68 (m, 2H, H-1'a, H-1'b). ^{13}C-NMR (75 MHz, $CDCl_3$): δ 166.2, 165.6, 165.5, 165.4, (4 × CO), 148.9 (Carom-N), 137.3, 135.0, 133.5, 133.4, 133.3, 133.0, 131.3, 129.8, 129.7, 128.9, 128.5, 127.7, 126.5, 125.2 (Carom, C-3', C-2'), 74.5 (C-1), 70,4 (C-5), 69.1 (C-4), 67.8 (C-3), 66.0 (C-2), 62.8 (C-6), 33.3 (C-1'). ESI$^+$-HRMS: $[M + H]^+$: calcd for $C_{48}H_{40}NO_9$, 774.26; found, 774.2690.

Compound **19** was deprotected according to general procedure above to afford compound **20**: 7 mg, 0.02 mmol, 80%, $[\alpha]^{20}_{D}$ = +17.38 (*c* = 0.13, CH_3OH). ^{1}H-NMR (300 MHz, CD_3OD): δ 8.61 (s, 2H, Harom), 7.69 (d, 1H, $^3J_{H-H}$ = 7.9 Hz, H-arom), 7.49–7.29 (m,

5H, $^{3}J_{H\text{-}H}$ = 7.9 Hz, H-arom), 6.43 (d, 1H, $J_{2',3'}$ = 15.7 Hz, CH=C<u>H</u>Ph), 6.33–6.14 (m, 1H, C<u>H</u>=CHPh), 4.04–3.91 (m, 1H, H-1), 3.83–3.62 (m, 5H, H-4, H-3, H-2, H-6a,H-6b) 3.5–3.47 (m, 1H, H-5), 2.69–2.51 (m, 1H, H-1'a), 2.50–2.38 (m, 1H, H-1'b). ^{13}C-NMR (151 MHz, CD_3OD): δ, 148.6, 136.9, 135.4, 129.9 (Carom), 129.1 (C-2'), 128.7, 128.6 (C-3'), 128.0, 127.2, 126.3, 125.1 (Carom), 76.5 (C-1), 74,8 (C-5), 71.1 (C-4), 70.6 (C-3), 68.9 (C-2), 61.7 (C-6), 32.5 (C-1'). ESI$^+$-HRMS: $[M + H]^+$: calcd for $C_{20}H_{24}NO_5$, 357.16; found, 357.1666.

3.3. Bioactivity Assay

3.3.1. Expression and Purification of FimH

The FimH lectin (Phe1-Thr158) was produced and purified as described previously [46] by expression from the pET-24a vector in *E. coli* C43(DE3) [45] in MinA medium complemented with the 20 amino acids, the vitamins biotin and thiamin, glucose and $MgCl_2$. Soluble FimH lectin secreted in the periplasm was extracted by applying 30% sucrose and 2.5 mM EDTA, in 20 mM HEPES at pH 7.4, onto the washed bacterial pellet followed by a 30-fold dilution in the same buffer to cause the desired osmotic shock. A 30' centrifugation at 13,000× *g* was carried out to eliminate the cellular debris present in the pellet and isolate the soluble proteins in the supernatant. The supernatant was acidified using HCl to pH = 3.9 and centrifuged again before cation exchange chromatography onto an HiTrap Sulfopropyl Fast Flow column (SPFF, Cytiva). The SPFF column was washed in 20 mM formic acid (pH = 3.9) and eluted using a salt gradient. The fractions containing FimH lectin eluted between 150–250 mM NaCl and were immediately neutralized upon elution by adding a drop of 1 M HEPES at pH 7.4. Finally, pure protein fractions were pooled and dialyzed against 20 mM HEPES at pH 7.4 containing 150 mM NaCl.

3.3.2. Co-Crystallization of Antagonist **11** with FimH

Purified FimH lectin was concentrated to 17.19 mg·mL^{-1} and 1 mM of ligand **11** was added for co-crystallization at 20 °C using the sitting-drop vapor-diffusion method. A single crystal was obtained in a condition from the JCSG crystallization screen (Molecular Dimensions), containing 3.0 M NaCl and 0.1 M BIS-TRIS at pH = 5.5 (Figure S5). Cryoprotection prior to flash-freezing in liquid nitrogen was performed by dragging the crystal through a drop containing 3.5 M NaCl, 50 mM BIS-TRIS at pH 5.5 and 30% glycerol. The crystal diffracted to 3 Å resolution at the PX1 beamline of the French Soleil synchrotron. Molecular replacement using PDB entry 2VCO (same as above) [46] of its oligomannose-3 ligands, led to the placement of four FimH lectin protomers in the unit cell of the hexagonal crystal. Iterative rounds of refinements were performed using PHENIX and the model was adjusted manually using Coot [56]. The crystal structure was run through PDB_REDO [57], for further optimization, and validated using Molprobity [58] and Staraniso [59].

3.3.3. Affinity Evaluation of Mannosides through FimH LEctPROFILE Kit

FimH LEctPROFILE kit assays from GLYcoDiag (Orléans, France) were performed according to GlycoDiag's protocol already described [60–62]. Briefly, the interaction profiles of each compound were determined through a competitive inhibition assay based on the inhibition by the compounds of the interaction between FimH lectin coated onto the microplate surface and a biotinylated neoglycoprotein NeoM (Man-BSA) as a tracer. A mix of biotinylated Man-BSA (fixed concentration) and the corresponding compounds (range of concentrations) prepared in PBS supplemented with 1 mM $CaCl_2$ and 0.5 mM $MgCl_2$ was deposited in each well (50 µL each) in triplicate and incubated for two hours at room temperature. After washing with PBS buffer, the conjugate streptavidin-DTAF (dichlorotriazinylamino fluorescein) was added (50 µL) and incubated 30 min more. The plate was washed again with PBS. Finally, 100 µL of PBS was added for the readout of fluorescent plate performed with a fluorescence reader (Pherastar microplate reader, BMG labtech, λex = 485 nm, λem = 530 nm). The signal intensity is inversely correlated with the capacity of the compound to be recognized by the lectin and expressed as inhibition percentage with comparison with the corresponding tracer alone. Data analysis was performed with

GraphPadPrism software (version 5.03 for windows, San Diego, CA, USA). 50% inhibitory concentration (IC_{50}) was determined according to a standard dose-response/inhibition fitting model with the following equation: y = 100 / (1 + [inhibitor]/IC_{50}) and expressed in nanomolar units.

3.3.4. Bacterial Strains and Cell Line

The well characterized UPEC strain CFT073 (ATCC 700928) was used as the uropathotype in this study. Strain CFT073 was grown at 37 °C in LB or seeded onto MacConkey agar plates. The presence of the *fimH* gene was confirmed by PCR using the primers fimH-F 5′-TGCAGAACGGATAAGCCGTGG-3′ and fimH-R 5′-GCAGTCACCTGCCCTCCGGTA-3′ and *E. coli fimH*-proficient and -deficient strains served as positive and negative controls (E1P and I2P strains), respectively [5,63,64]. The human bladder epithelial cell line 5637, (ATCC HTB-9) (ATCC-LGC, Milan, Italy) was routinely cultured in T25 flasks at 37 °C in a humidified atmosphere with 5% CO_2 using Roswell Park Memorial Institute (RPMI) 1640 medium supplemented with 10% FBS (both Gibco, Milan, Italy).

3.3.5. Effect of Mannosides on Bacterial Growth and Metabolism

Mannosides dissolved in dimethyl sulfoxide DMSO or water at a final concentration of 5 mM were prepared. To test the mannosides' toxicity, strain CFT073 was grown on LB medium supplemented with each molecule reported in Table 1, at a final concentration of 50, 100 and 500 µM. Natural D-mannose (D-Man) at equal concentration to the mannosides was used as control. LB supplemented with DMSO was included as growth control. Bacterial cultures were then incubated in a 96-well plate at 37 °C over a period of 10 h with a 30 min temperature equilibration period before data acquisition started. Readings of culture turbidity (OD_{600}) were determined using a plate reader (POLARstar Omega BMG Labtech plate reader, Germany). To evaluate whether mannosides could be used as carbon sources, an initial inoculum of strain CFT073 of ~1.5 × 10^7 CFU/mL was incubated in PBS supplemented with each molecule at a final concentration of 500 µM for 24 h at 37 °C. Following incubation, the growth of strain CFT073 was determined by colony forming unit (CFU/mL) counting by spot-plating serial dilutions.

3.3.6. Cell Viability and Toxicity Assay

To evaluate whether synthesized mannosides can affect eukaryotic cells viability, HTB-9 cells were seeded onto 24-well plates at 5 × 10^5 cells per mL and incubated in RPMI supplemented with 10% FBS in the presence of each mannoside molecule at a final concentration of 50, 100 and 500 µM at 37 °C in a 5% CO_2 atmosphere for 24 h. At this point, cell viability was determined by the MTT assay. The medium was replaced by fresh RPMI supplemented with 10% FBS and 1 mg/mL MTT, and the cells were further incubated for 1 h. Viable cells, with active metabolism able to metabolize yellow tetrazole (MTT) into purple formazan crystals, were quantified by measuring the absorbance at 570 nm of formazan crystals formed and solubilized with isopropanol.

3.3.7. Antibiotic-Mannoside Interference Assay

To assess any interference with antibiotic activities, strain CFT073 (approximately 10^5–10^6 CFU/well) was inoculated into a 96-well microplate supplemented with LB containing ampicillin (AMP 30 µg/mL), streptomycin (SM 50 µg/mL) and gentamycin (GM 50 µg/mL) with or without the addition of each mannoside antagonist (500 µM concentration). LB supplemented with DMSO was included as growth control in this experiment. The microplate was incubated at 37 °C and bacterial growth kinetics were monitored by measuring the OD_{600} over a period of 16 h.

3.3.8. Bacterial Adhesion Assay

HTB-9 cells were routinely seeded in cell culture plates and maintained 2–4 days at 37 °C in a humidified atmosphere containing 5% CO_2. For the adhesion assay, cells were

seeded in 35 mm tissue culture plates at a density of 1×10^5 cells/well and incubated at 37 °C for 48 h to reach confluency. CFT073 was grown in LB under mild shaking conditions overnight and resuspended in phosphate buffer (PBS) to an inoculum of ~10^6 CFU/mL (normalized according to OD_{600}). Each mannoside molecule was added to CFT073 inoculant at the final concentrations of 100, 500 µM and 1 mM and incubated for 3 h in static conditions. One ml of these bacterial/mannosides mixtures was used to infect HTB-9 cell monolayers at a multiplicity of infection (MOI) of 10; monolayers were centrifuged (10′ at 2000× *g*) and incubated at 37 °C with 5% CO_2 for 2.5 h. The CFT073 strain incubated without any mannoside molecules was used as control. Monolayers were extensively washed (seven times) with PBS and lysed with 0.1% Triton X-100 in PBS. Cell lysates were serially diluted and spot-plated onto LB agar plates for CFU/mL counting. Parallel infected cells were Giemsa stained for qualitative assessment of bacterial adhesion, as previously described [5,65]. Images were recorded with a Leica DM5000B microscope equipped with DFX340/DFX300 camera and processed using the Leica Application Suite 2.7.0.R1 software (Leica).

3.3.9. Molecular Dynamics Simulations

The complex of compound **20** and the FimH lectin domain (a.a. 1-158) with the best score using induced fit was used as the starting configuration for the molecular dynamics (MD) simulations. The complex was solvated and the structural waters were added using the same structural information as in the docking (PDB code: 4AUY) [66] and the ionic concentration was set to 0.15 M NaCl. In accordance with propKa [67] the standard protonation state at pH 7 was used for all protonatable groups of FimH. The generated molecular system comprised about 45,000 atoms including around 15,000 water molecules. The CHARMM36 force field with CMAP corrections was used to describe protein, water, and ion atoms [68–70]. Missing force field parameters for compound **20** were initially generated with CGenFF [68] with standard parameters and afterwards adapted. The integrity of the compound was verified in a 50-ns long MD simulation of the compound alone in water using the adapted force field.

Two independent simulations of the so generated system were performed. In each of them a three-step equilibration was applied: first, a 2.5 ns long equilibration of the water and ions molecules, second a 2.5 ns long equilibration in which only the protein backbone was fixed, and third unrestrained simulations was carried out for 2.5 ns. This was followed by a 30-ns long production run.

All MD calculations were performed in the isothermal-isobaric ensemble at 300 K with the program NAMD2.9 [48]. Long-range electrostatic interactions were calculated using the particle-mesh Ewald method [49]. A smoothing function was applied to truncate short-range electrostatic interactions. The Verlet-I/r-RESPA multiple time-step propagator [51] was used to integrate the equation of motions using a time step of 2 and 4 fs for short- and long-range forces, respectively. All bonds involving hydrogen atoms were constrained using the Rattle algorithm [50].

4. Conclusions

In this study, the design, synthesis, and function of a small library of *C*-mannose inhibitors containing heteroaryl moieties were reported. Their relative binding affinity was measured using a competitive inhibition assay against the binding of FimH with mannosylated BSA conjugate. Among them, the best results were obtained with compounds **20** and **11**, respectively. Although compound **20** had a higher inhibitory potency (IC_{50} 0.82 ± 0.4) against isolated FimH lectin binding domain, ligand **11** (IC_{50} 3.17 ± 2.3) showed better potency in inhibiting bacterial adhesion to bladder HTB-9 cell monolayers without adverse side effects. The crystal structure of the FimH lectin-binding domain co-crystallized with inhibitor **11** was obtained at a resolution of 3 Å. It also confirmed the expected $^4C_1$ chair conformation of antagonist **11** bound into the active site of the tyrosine gate. Interestingly, the inter-molecular π-π stacking of two quinolines residues of **11** triggered the interlacing

of two FimH lectins, providing a "bidentate" complex. Furthermore, in the mannose-binding site between FimH and ligand **11**, Tyr48 was shown to be p-stacked in parallel to the quinoline moiety, while its Tyr137 appeared to form T-aromatic stacking. On the other hand, molecular dynamics (MD) simulations were done for the best antagonist **20**, which unfortunately failed to provide co-crystals with FimH. The results indicated that the lowest potential energy was obtained with the FimH in its *half-open* conformation. The docking of compound **20** to this conformer helped raising the hypothesis that its high affinity may originate from a p-stacking of the first phenyl ring with Tyr48, as well as from the interaction of the *ortho*-pyridyl moiety with Tyr137 through a potential hydrogen bond.

In addition, the synthetic *C*-linked mannopyranoside inhibitors discussed herein neither affected bacterial growth or cell viability, nor interfered with antibiotic activity. The latter aspect is particularly important because antibiotics still represent the standard treatment for UTIs. However, literature data evidenced the increase of the number of cleared infections when antibiotics were administrated in combination with D-mannose [71]. Moreover, the preventive use of D-mannose showed a reduced number of UTIs in patients suffering from rUTIs. Hence, the reported mannoside derivatives, and in particular molecules **11** and **20**, represent good candidates to be analyzed in clinical trials to definitively accelerate the inclusion of mannoside-based FimH inhibitors in the clinical guidelines for the treatment of UTIs.

Supplementary Materials: The following supporting information can be downloaded at: https://www.mdpi.com/article/10.3390/pharmaceutics15020527/s1, Figures S1–S3 related to D1, D2 and Noesy NMR structural analyses of compound **2**. Figure S4: ORTEP diagram of compound **2**, and Figure S5: ES. HRMS of compound **2**, Figures S6–S37: related to ^{1}HNMR, ^{13}CNMR, and ES. HRMS of compound **3** to **20**, S38: Co-crystal structure of FimH with the ligand **11**. Table S1: X-ray data collection and refinement statistics.; and Figure S39: a perform serial dilution of FimH with ligands.

Author Contributions: Conceptualization, L.M. and R.R.; methodology, L.M., M.S., C.B., B.R., D.S., C.A., A.T.P., G.V., L.L. and B.R.; validation, L.M., J.B. and R.R.; formal analysis, L.M., J.B. and R.R.; investigation, L.M., M.S., C.B., B.R., D.S., C.A., A.T.P.,G.V., L.L. and B.R.; resources, J.B. and R.R.; data curation, L.M., M.S., C.B., B.R., D.S., C.A., A.T.P., L.L., B.R., J.B. and R.R.; writing—original draft preparation, L.M. and R.R.; writing—review and editing, L.M., M.S., C.B., B.R., D.S., C.A., A.T.P., L.L, B.R., J.B. and R.R.; visualization, L.M., M.S., C.B., B.R., D.S., C.A., A.T.P., G.V., L.L., B.R., J.B. and R.R.; supervision.; R.R.; project administration, L.M. and R.R.; funding acquisition, R.R. All authors have read and agreed to the published version of the manuscript.

Funding: This work was supported from Natural Sciences and Engineering Research Council of Canada (NSERC) Discovery Grant (Project Grant RGPIN-2018-05570) and a Canadian Research Chair in Therapeutic Chemistry (Grant CRC-202061) to R.R. This research was also supported by the Ricerca Corrente IRCCS San Raffaele Roma to C.A. and from Dani Di Giò Foundation-Onlus, Rome, Italy to D.S. Salary of D.S. and M.S. were supported by POR Lazio FSE 2014-2020 and Sapienza Ateneo fundings and by the Italian Ministry of Health (starting grant SG-2018-12365432), respectively.

Institutional Review Board Statement: Not applicable.

Informed Consent Statement: Not applicable.

Data Availability Statement: Not applicable.

Conflicts of Interest: The authors declare no conflict of interest. The funding sponsors had no role in the design of the study; in the collection, analyses, or interpretation of data; in the writing of the manuscript, and in the decision to publish the results.

References

1. Spaulding, C.N.; Klein, R.D.; Ruer, S.; Kau, A.L.; Schreiber, H.L.; Cusumano, Z.T.; Dodson, K.W.; Pinkner, J.S.; Fremont, D.H.; Janetka, J.W.; et al. Selective depletion of uropathogenic *E. coli* from the gut by a FimH antagonist. *Nature* **2017**, *546*, 528–532. [CrossRef]
2. Terlizzi, M.E.; Gribaudo, G.; Maffei, M.E. Uropathogenic *Escherichia coli* (UPEC) infections: Virulence factors, bladder responses, antibiotic, and non-antibiotic antimicrobial strategies. *Front. Microbiol.* **2017**, *8*, 1566. [CrossRef]

3. Abe, C.M.; Salvador, A.; Falsetti, I.N.; Blanco, E.; Blanco, M. Uropathogenic *Escherichia coli* (UPEC) strains may carry virulence properties of diarrhoeagenic *E. coli*. *FEMS Immunol. Med. Microbiol.* **2008**, *52*, 397–406. [CrossRef]
4. Mousavifar, L.; Touaibia, M.; Roy, R. Development of Mannopyranoside Therapeutics against Adherent-Invasive *Escherichia coli* Infections. *Acc. Chem. Res.* **2018**, *51*, 2937–2948. [CrossRef]
5. Scribano, D.; Sarshar, M.; Prezioso, C.; Lucarelli, M.; Angeloni, A.; Zagaglia, C.; Palamara, A.T.; Ambrosi, C. D-Mannose Treatment neither Affects Uropathogenic *Escherichia coli* Properties nor Induces Stable FimH Modifications. *Molecules.* **2020**, *25*, 316. [CrossRef]
6. Sarshar, M.; Behzadi, P.; Ambrosi, C.; Zagaglia, C. FimH and Anti-Adhesive Therapeutics: A Disarming Strategy Against Uropathogens. *Antibiotics.* **2020**, *9*, 397. [CrossRef]
7. Palmela, C.; Chevarin, C.; Xu, Z.; Torres, J.; Sevrin, G.; Hirten, R.; Barnich, N.; Ng, S.C.; Colombel, J.F. Adherent-invasive *Escherichia coli* in inflammatory bowel disease. *Gut* **2018**, *67*, 574–587. [CrossRef]
8. Wagenlehner, F.; Lorenz, H.; Ewald, O.; Gerke, P. Why D -Mannose May Be as Efficient as Antibiotics in the Treatment of Acute Uncomplicated Lower Urinary Tract Infections—Preliminary Considerations and Conclusions from a Non-Interventional Study. *Antibiotics* **2022**, *11*, 314. [CrossRef]
9. Hudson, R.E.; Job, K.M.; Sayre, C.L.; Krepkova, L.V.; Sherwin, C.M.; Enioutina, E.Y. Examination of Complementary Medicine for Treating Urinary Tract Infections Among Pregnant Women and Children. *Front. Pharmacol.* **2022**, *13*, 1541. [CrossRef]
10. Ohman, L.; Magnusson, K.E.; Stendahl, O. Effect OF Monosaccharides and Ethyleneglycol on the Interaction Between *Escherichia coli* Bacteria and Octyl-Sepharose. *Acta Path. Microbiol. Immunol. Scand. Sect. B* **1985**, *93*, 133–138.
11. Feenstra, T.; Thøgersen, M.S.; Wieser, E.; Peschel, A.; Ball, M.J.; Brandes, R.; Satchell, S.C.; Stockner, T.; Aarestrup, F.M.; Rees, A.J.; et al. Adhesion of *Escherichia coli* under flow conditions reveals potential novel effects of FimH mutations. *Eur. J. Clin. Microbiol. Infect. Dis.* **2017**, *36*, 467–478. [CrossRef]
12. Scaglione, F.; Musazzi, U.M.; Minghetti, P. Considerations on D-mannose Mechanism of Action and Consequent Classification of Marketed Healthcare Products. *Front. Pharmacol.* **2021**, *12*, 636377. [CrossRef] [PubMed]
13. Hatton, N.E.; Baumann, C.G.; Fascione, M.A. Developments in Mannose-Based Treatments for Uropathogenic *Escherichia coli* -Induced Urinary Tract Infections. *Chembiochem* **2021**, *22*, 613–629. [CrossRef] [PubMed]
14. Mousavifar, L.; Roy, R. Recent development in the design of small ' drug-like ' and nanoscale glycomimetics against *Escherichia coli* infections. *Drug Discov. Today.* **2021**, *26*, 2124–2137. [CrossRef]
15. Mydock-McGrane, L.K.; Cusumano, Z.T.; Janetka, J.W. Mannose-derived FimH antagonists: A promising anti-virulence therapeutic strategy for urinary tract infections and Crohn's disease. *Expert Opin. Ther. Pat.* **2016**, *26*, 175–197. [CrossRef]
16. Pang, L.; Kleeb, S.; Lemme, K.; Rabbani, S.; Scharenberg, M.; Zalewski, A.; Schädler, F.; Schwardt, O.; Ernst, B. FimH Antagonists: Structure-Activity and Structure-Property Relationships for Biphenyl α-D-Mannopyranosides. *ChemMedChem* **2012**, *7*, 1404–1422. [CrossRef]
17. Sivignon, A.; Yan, X.; Dorta, D.A.; Bonnet, R.; Bouckaert, J.; Fleury, E.; Bernard, J.; Gouin, S.G.; Darfeuille-Michaud, A.; Barnich, N. Development of heptylmannoside-based glycoconjugate antiadhesive compounds against adherent-invasive *Escherichia coli* bacteria associated with crohn's disease. *MBio* **2015**, *6*, e01298-15. [CrossRef]
18. Bouckaert, J.; Mackenzie, J.; de Paz, J.L.; Chipwaza, B.; Choudhury, D.; Zavialov, A.; Mannerstedt, K.; Anderson, J.; Piérard, D.; Wyns, L.; et al. The affinity of the FimH fimbrial adhesin is receptor-driven and quasi-independent of *Escherichia coli* pathotypes. *Mol. Microbiol.* **2006**, *61*, 1556–1568. [CrossRef]
19. Touaibia, M.; Wellens, A.; Tze, C.S.; Wang, Q.; Sirois, S.; Bouckaert, J.; Roy, R. Mannosylated G(0) dendrimers with nanomolar affinities to *Escherichia coli* FimH. *ChemMedChem* **2007**, *2*, 1190–1201. [CrossRef]
20. Bernardi, A.; Jiménez-Barbero, J.; Casnati, A.; De Castro, C.; Darbre, T.; Fieschi, F.; Finne, J.; Funken, H.; Jaeger, K.E.; Lahmann, M.; et al. Multivalent glycoconjugates as anti-pathogenic agents. *Chem. Soc. Rev.* **2013**, *42*, 4709–4727. [CrossRef]
21. Lindhorst, T.K.; Dubber, M.; Krallmann-Wenzel, U.; Ehlers, S. Cluster Mannosides as Inhibitors of Type 1 Fimbriae-Mediated Adhesion of *Escherichia coli*: Pentaerythritol Derivatives as Scaffolds. *Eur. J. Org. Chem.* **2000**, *2000*, 2027–2034. [CrossRef]
22. Twibanire, J.A.K.; Paul, N.K.; Grindley, T.B. Synthesis of novel types of polyester glycodendrimers as potential inhibitors of urinary tract infections. *New J. Chem.* **2015**, *39*, 4115–4127. [CrossRef]
23. Almant, M.; Moreau, V.; Kovensky, J.; Bouckaert, J.; Gouin, S.G. Clustering of *Escherichia coli* type-1 fimbrial adhesins by using multimeric heptyl α- D -mannoside probes with a carbohydrate core. *Chem.-A Eur. J.* **2011**, *17*, 10029–10038. [CrossRef]
24. Bouckaert, J.; Li, Z.; Xavier, C.; Almant, M.; Caveliers, V.; Lahoutte, T.; Weeks, S.D.; Kovensky, J.; Gouin, S.G. Heptyl a-D-Mannosides Grafted on a b-Cyclodextrin Core to Interfere with *Escherichia coli* Adhesion: An *In Vivo* Multivalent Effect. *Chem. Eur. J.* **2013**, *19*, 7847–7855. [CrossRef] [PubMed]
25. Yan, X.; Sivignon, A.; Yamakawa, N.; Crepet, A.; Travelet, C.; Borsali, R.; Dumych, T.; Li, Z.; Bilyy, R.; Deniaud, D.; et al. Glycopolymers as Antiadhesives of *E. coli* Strains Inducing In fl ammatory Bowel Diseases. *Bio Mac.* **2015**, *16*, 1827–1836. [CrossRef]
26. Schwardt, O.; Rabbani, S.; Hartmann, M.; Abgottspon, D.; Wittwer, M.; Kleeb, S.; Zalewski, A.; Smieško, M.; Cutting, B.; Ernst, B. Design, synthesis and biological evaluation of mannosyl triazoles as FimH antagonists. *Bioorg. Med. Chem* **2011**, *19*, 6454–6473. [CrossRef] [PubMed]
27. Tomašić, T.; Rabbani, S.; Gobec, M.; Raščan, I.M.; Podlipnik, Č.; Ernst, B.; Anderluh, M. Branched a-D-mannopyranosides: A new class of potent FimH antagonists. *Med. Chem. Commun.* **2014**, *5*, 1247–1253. [CrossRef]

28. Vetterli, S.U.; Moehle, K.; Robinson, J.A. Synthesis and antimicrobial activity against Pseudomonas aeruginosa of macrocyclic b -hairpin peptidomimetic antibiotics containing N -methylated amino acids. *Bioorg. Med. Chem.* **2016**, *24*, 6332–6339. [CrossRef]
29. Han, Z.; Pinkner, J.S.; Ford, B.; Obermann, R.; Nolan, W.; Wildman, S.A.; Hobbs, D.; Ellenberger, T.; Cusumano, C.K.; Hultgren, S.J.; et al. Structure-based drug design and optimization of mannoside bacterial fimH antagonists. *J. Med. Chem.* **2010**, *53*, 4779–4792. [CrossRef]
30. Mousavifar, L.; Vergoten, G.; Charron, G.; Roy, R. Comparative Study of Aryl O-, C-, and S-Mannopyranosides as potential Adhesion Inhibitors toward Uropathogenic E. coli FimH. *Molecules.* **2019**, *24*, 3566. [CrossRef]
31. Krammer, E.M.; De Ruyck, J.; Roos, G.; Bouckaert, J.; Lensink, M.F. Targeting dynamical binding processes in the design of non-antibiotic anti-adhesives by molecular simulation—The example of FimH. *Molecules* **2018**, *23*, 1641. [CrossRef] [PubMed]
32. Alvarez Dorta, D.; Sivignon, A.; Chalopin, T.; Dumych, T.I.; Roos, G.; Bilyy, R.O.; Deniaud, D.; Krammer, E.M.; De Ruyck, J.; Lensink, M.F.; et al. The Antiadhesive Strategy in Crohn's Disease: Orally Active Mannosides to Decolonize Pathogenic *Escherichia coli* from the Gut. *ChemBioChem* **2016**, *17*, 936–952. [CrossRef] [PubMed]
33. Chalopin, T.; Dorta, D.A.; Sivignon, A.; Caudan, M.; Dumych, T.I.; Bilyy, R.O.; Deniaud, D.; Barnich, N.; Bouckaert, J.; Gouin, S.G. Second generation of thiazolylmannosides, FimH antagonists for E. coli-induced Crohn's disease. *Org. Biomol. Chem.* **2016**, *14*, 3913–3925. [CrossRef]
34. Brument, S.; Sivignon, A.; Dumych, T.I.; Moreau, N.; Roos, G.; Guérardel, Y.; Gouin, S.G. Thiazolylaminomannosides As Potent Antiadhesives of Type 1 Piliated *Escherichia coli* Isolated from Crohn' s Disease Patients. *J. Med. Chem.* **2013**, *56*, 5395–5406. [CrossRef] [PubMed]
35. Han, Z.; Pinkner, J.S.; Ford, B.; Chorell, E.; Crowley, J.M.; Cusumano, C.K.; Campbell, S.; Henderson, J.P.; Hultgren, S.J.; Janetka, J.W. Lead optimization studies on FimH antagonists: Discovery of potent and orally bioavailable ortho-substituted biphenyl mannosides. *J. Med. Chem.* **2012**, *55*, 3945–3959. [CrossRef]
36. Mydock-McGrane, L.K.; Hannan, T.J.; Janetka, J.W. Rational Design Strategies for FimH Antagonists: New Drugs on the Horizon for Urinary Tract Infection and Crohn's Disease. *Expert Opin. Drug Discov.* **2017**, *12*, 711–731. [CrossRef]
37. Huggins, D.J.; Sherman, W.; Tidor, B. Rational approaches to improving selectivity in drug design. *J. Med.Chem.* **2012**, *55*, 1424–1444. [CrossRef]
38. Toma, T.; Maier, T.; Ernst, B.; Anderluh, M. Does targeting Arg98 of FimH lead to high af fi nity antagonists? *Eur. J. Med. Chem.* **2021**, *211*, 113093. [CrossRef]
39. Mydock-McGrane, L.; Cusumano, Z.; Han, Z.; Binkley, J.; Kostakioti, M.; Hannan, T.; Pinkner, J.S.; Klein, R.; Kalas, V.; Crowley, J.; et al. Antivirulence C-Mannosides as Antibiotic-Sparing, Oral Therapeutics for Urinary Tract Infections. *J. Med. Chem.* **2016**, *59*, 9390–9408. [CrossRef]
40. Mousavifar, L.; Vergoten, G.; Roy, R. Deciphering the conformation of C -linked α-D-mannopyranosides and their application toward the synthesis of low nanomolar *E. coli* FimH ligands. *ARKIVOC Free. Online J. Org. Chem.* **2018**, *2018*, 384–397. [CrossRef]
41. Touaibia, M.; Krammer, E.-M.; Shiao, T.C.; Yamakawa, N.; Wang, Q.; Glinschert, A.; Papadopoulos, A.; Mousavifar, L.; Maes, E.; Oscarson, S.; et al. Sites for dynamic protein-carbohydrate interactions of O- and C-linked mannosides on the *E. coli* FimH adhesin. *Molecules* **2017**, *22*, 1101. [CrossRef]
42. Thakur, A.; Zhang, K.; Louie, J. Suzuki-Miyaura coupling of heteroaryl boronic acids and vinyl chlorides. *Chem. Commun.* **2012**, *48*, 203–205. [CrossRef]
43. Suzuki, A. Recent advances in the cross-coupling reactions of organoboron derivatives with organic electrophiles, 1995–1998. *J. Organomet. Chem.* **1999**, *576*, 147–168. [CrossRef]
44. Liebschner, D.; Afonine, P.V.; Baker, M.L.; Bunkóczi, G.; Chen, V.B.; Croll, T.I.; Hintze, B.; Hung, L.W.; Jain, S.; McCoy, A.J.; et al. Macromolecular structure determination using X-rays, neutrons and electrons: Recent developments in Phenix. *Acta Crystallogr. Sect. D Struct. Biol.* **2019**, *D75*, 861–877. [CrossRef]
45. Miroux, B.; Walker, J.E. Over-production of Proteins in *Escherichia coli*: Mutant Hosts that Allow Synthesis of some Membrane Proteins and Globular Proteins at High Levels. *J. Mol. Biol.* **1996**, *260*, 289–298. [CrossRef] [PubMed]
46. Wellens, A.; Garofalo, C.; Nguyen, H.; Van Gerven, N.; Slättegard, R.; Hernalsteens, J.P.; Wyns, L.; Oscarson, S.; De Greve, H.; Hultgren, S.; et al. Intervening with urinary tract infectious using anti-adhesives based on the crystal structure of the FimH-oligomannose-3 complex. *PLoS ONE* **2008**, *3*, e2040. [CrossRef]
47. Sauer, M.M.; Jakob, R.P.; Luber, T.; Canonica, F.; Ernst, B.; Unverzagt, C.; Maier, T.; Glockshuber, R. Binding of the bacterial adhesin FimH to its natural, multivalent high-mannose type glycan targets Binding of the bacterial adhesin FimH to its natural, multivalent high- mannose type glycan targets. *J. Am. Chem. Soc.* **2018**, *141*, 936–944. [CrossRef]
48. Phillips, J.C.; Braun, R.; Wang, W.; Gumbart, J.; Tajkhorshid, E.; Villa, E.; Chipot, C.; Skeel, R.D.; Kalé, L.; Schulten, K. Scalable molecular dynamics with NAMD. *J. Comput. Chem.* **2005**, *26*, 1781–1802. [CrossRef]
49. Darden, T.; York, D.; Pedersen, L. Particle mesh Ewald:An N*log(N) method for Ewald sums in large systems. *J. Chem. Phys.* **1993**, *98*, 10089–10092. [CrossRef]
50. Andersen, H.C. Rattle: A "velocity" version of the shake algorithm for molecular dynamics calculations. *J. Comput. Phys.* **1983**, *52*, 24–34. [CrossRef]
51. Tuckerman, M.; Berne, B.J.; Martyna, G.J. Reversible multiple time scale molecular dynamics. *J. Chem. Phys.* **1992**, *97*, 1990. [CrossRef]

52. Hung, C.S.; Bouckaert, J.; Hung, D.; Pinkner, J.; Widberg, C.; DeFusco, A.; Auguste, C.G.; Strouse, R.; Langermann, S.; Waksman, G.; et al. Structure basis of tropism of *Escherichia coli* to the bladder during urinary tract infection. *Mol. Microbiol.* **2002**, *44*, 903–915. [CrossRef]
53. Bianco, A.; Cavarischia, C.; Guiso, M. Total synthesis of anthocyanidins via Heck reaction. *Nat. Prod. Res.* **2006**, *20*, 93–97. [CrossRef]
54. Lindgren, A.E.G.; Öberg, C.T.; Hillgren, J.M.; Elofsson, M. Total synthesis of the resveratrol oligomers (±)-Ampelopsin B and (±)-σ-Viniferin. *Eur. J. Org. Chem.* **2016**, *2016*, 426–429. [CrossRef]
55. Cabrera-Afonso, M.J.; Lu, Z.P.; Kelly, C.B.; Lang, S.B.; Dykstra, R.; Gutierrez, O.; Molander, G.A. Engaging Sulfinate Salts via Ni/Photoredox Dual Catalysis Enables Facile C–SO_2R Coupling María. *Chem. Sci.* **2018**, *9*, 3186–3191. [CrossRef] [PubMed]
56. Emsley, P.; Cowtan, K. Coot: Model-building tools for molecular graphics research papers. *Acta Crystallogr. Sect. D Biol. Crystallogr.* **2004**, *60*, 2126–2132. [CrossRef] [PubMed]
57. Joosten, R.P.; Long, F.; Murshudov, G.N.; Perrakis, A. The PDB_REDO server for macromolecular structure model optimization. *IUCrJ* **2014**, *1*, 213–220. [CrossRef]
58. Williams, C.J.; Headd, J.J.; Moriarty, N.W.; Prisant, M.G.; Videau, L.L.; Deis, L.N.; Verma, V.; Keedy, D.A.; Hintze, B.J.; Chen, V.B.; et al. MolProbity: More and better reference data for improved all-atom structure validation. *Protein Sci.* **2018**, *27*, 293–315. [CrossRef]
59. Vonrhein, C.; Tickle, I.J.; Flensburg, C.; Keller, P.; Paciorek, W.; Sharff, A.; Bricogne, G. Advances in automated data and processing within autoPROC, combined with improved characterization, mitigation, and visualization of the anisotropy of diffraction limits using STARANISO. *Acta Crystallogr. Sect. A* **2018**, *74*, a360. [CrossRef]
60. Cauwel, M.; Sivignon, A.; Bridot, C.; Nongbe, M.C.; Deniaud, D.; Roubinet, B.; Landemarre, L. Heptylmannose-functionalized cellulose for the binding and specific detection of pathogenic *E. coli*. *Chem. Commun.* **2019**, *55*, 10158–10161. [CrossRef]
61. Landemarre, L.; Duverger, E. Lectin glycoprofiling of recombinant therapeutic interleukin-7. In *Glycosylation Engineering of Biopharmaceuticals. Methods in Molecular Biology*; Alain beck, Ed.; Humana Press of Springer Science: Totowa, NJ, USA, 2013; pp. 221–226, ISBN 9781627033268.
62. Brissonnet, Y.; Compain, G.; Renoux, B.; Krammer, E.; Daligault, F.; Deniaud, D. Monitoring glycosidase activity for clustered sugar substrates, a study on b -glucuronidase. *RSC Adv.* **2019**, *9*, 40263–40267. [CrossRef]
63. Sarshar, M.; Scribano, D.; Marazzato, M.; Ambrosi, C.; Rita, M.; Aleandri, M.; Pronio, A.; Longhi, C.; Nicoletti, M.; Zagaglia, C.; et al. Genetic diversity, phylogroup distribution and virulence gene pro fi le of pks positive *Escherichia coli* colonizing human intestinal polyps. *Microb. Pathog.* **2017**, *112*, 274–278. [CrossRef]
64. Ambrosi, C.; Sarshar, M.; Rita, M.; Pompilio, A.; Di, G.; Strati, F.; Pronio, A.; Nicoletti, M.; Zagaglia, C.; Teresa, A.; et al. Colonic adenoma-associated *Escherichia coli* express speci fi c phenotypes. *Microbes Infect.* **2019**, *21*, 305–312. [CrossRef]
65. Ambrosi, C.; Pompili, M.; Scribano, D.; Zagaglia, C.; Ripa, S.; Nicoletti, M. Outer Membrane Protein A (OmpA): A New Player in Shigella flexneri Protrusion Formation and Inter-Cellular Spreading. *PLoS ONE* **2012**, *7*, e49625. [CrossRef]
66. Wellens, A.; Lahmann, M.; Touaibia, M.; Vaucher, J.; Oscarson, S.; Roy, R.; Remaut, H.; Bouckaert, J. The tyrosine gate as a potential entropic lever in the receptor-binding site of the bacterial adhesin FimH. *Biochemistry* **2012**, *51*, 4790–4799. [CrossRef]
67. Bas, D.C.; Rogers, D.M.; Jensen, J.H. Very fast prediction and rationalization of pKa values for protein-ligand complexes. *Proteins* **2008**, *73*, 765–783. [CrossRef]
68. Vanommeslaeghe, K.; Hatcher, E.; Acharya, C.; Kundu, S.; Zhong, S.; Shim, J.; Darian, E.; Guvench, O.; Lopes, P.; Vorobyov, I.; et al. CHARMM general force field: A force field for drug-like molecules compatible with the CHARMM all-atom additive biological force fields. *J. Comput. Chem.* **2010**, *31*, 671–690. [CrossRef]
69. MacKerell, A.D.; Bashford, D.; Bellott, M.; Dunbrack, R.L.; Evanseck, J.D.; Field, M.J.; Fischer, S.; Gao, J.; Guo, H.; Ha, S.; et al. All-atom empirical potential for molecular modeling and dynamics studies of proteins. *J. Phys. Chem. B* **1998**, *102*, 3586–3616. [CrossRef]
70. MacKerell, A.D.; Feig, M.; Brooks, C.L. Extending the treatment of backbone energetics in protein force fields: Limitations of gas-phase quantum mechanics in reproducing protein conformational distributions in molecular dynamics simulations. *J. Comput. Chem.* **2004**, *25*, 1400–1415. [CrossRef]
71. De Nunzio, C.; Bartoletti, R.; Tubaro, A.; Simonato, A. Role of D-Mannose in the Prevention of Recurrent Uncomplicated Cystitis: State of the Art and Future Perspectives. *Antibiotics* **2021**, *10*, 373. [CrossRef]